

Chapter 2

Replication Stress by Py-Im Polyamides

Induces a Non-canonical ATR-dependent Checkpoint Response

The text of this chapter was taken in part from a manuscript co-authored with John W. Phillips, Kenneth K. Karanja, Piotr Polazcek, Chieh-Mei Wang, Benjamin C. Li, Judith L. Campbell, and Peter B. Dervan (California Institute of Technology)

(Martinez, T.F., Phillips, J.W., Karanja, K.K., Polazcek, P., Wang, C.M., Li, B.C., Campbell, J.L. and Dervan, P.B. (2014) Replication stress by Py-Im polyamides induces a non-canonical ATR-dependent checkpoint response. *Nucleic Acids Res*, 42, 11546-11559.)

Abstract

Pyrrrole-imidazole polyamides targeted to the androgen response element were cytotoxic in multiple cell lines, independent of intact androgen receptor signaling. Polyamide treatment induced accumulation of S-phase cells and of PCNA replication/repair foci. Activation of a cell cycle checkpoint response was evidenced by autophosphorylation of ATR, the S-phase checkpoint kinase, and by recruitment of ATR and the ATR activators RPA, 9-1-1, and Rad17 to chromatin. Surprisingly, ATR activation was accompanied by only a slight increase in single-stranded DNA, and the ATR targets RPA2 and Chk1, a cell cycle checkpoint kinase, were not phosphorylated. However, ATR activation resulted in phosphorylation of the replicative helicase subunit MCM2, an ATR effector. Polyamide treatment also induced accumulation of monoubiquitinated FANCD2, which is recruited to stalled replication forks and interacts transiently with phospho-MCM2. This suggests that polyamides induce replication stress that ATR can counteract independently of Chk1 and that the FA/BRCA pathway may also be involved in the response to polyamides. In biochemical assays, polyamides inhibit DNA helicases, providing a plausible mechanism for S-phase inhibition.

2.1 Introduction

Many DNA-binding small molecules can challenge a cell's ability to accurately replicate its DNA. Tolerance to various forms of replication stress is possible with the aid of stress sensors and mediators that activate DNA repair and cell cycle pathways, collectively called the DNA damage response (DDR) (1). The master regulators of the DDR are ATR and ATM, two PI3 protein kinase family members which respond to stalled replication forks and DNA breaks. ATR and ATM phosphorylate many substrates to stabilize the DNA replication fork and activate cell cycle checkpoints. The checkpoints slow cell cycle progression and allow time for the cell to respond to stress before entry into mitosis (2). During S-phase, ATR is recruited to sites of stalled replication by RPA-bound single-stranded DNA (ssDNA) in the presence of DNA damage. ATR is activated by a complex of many proteins and phosphorylates a number of targets, among which Chk1, a cell cycle checkpoint kinase, is best understood (3,4). ATM is similarly recruited to sites of double stranded breaks (DSBs) by the Mre11-Rad50-NBS1 (MRN) complex, where it can phosphorylate Chk2, another cell cycle checkpoint kinase, and the histone variant H2AX (5). However, how the DDR reacts to specific types of stresses, what downstream signaling events are necessary, and what physical structures are sensed are still under investigation (6). Furthermore, there are many levels of crosstalk between ATM and ATR and many targets beyond the checkpoint kinases, Chk1 and Chk2, which adds to the complexity (4). We have studied the checkpoint response activated by DNA minor groove binding pyrrole-imidazole (Py-Im) polyamides to discover what response polyamides elicit.

Py-Im polyamides are programmable small molecules that bind in the minor groove of double-stranded DNA with affinities and specificities comparable to DNA-binding proteins (7,8). Binding of the polyamides alters the local helical structure of DNA (9). Eight-ring hairpin polyamides are cell-permeable and localize to the nucleus in live cells (10). Py-Im Polyamides are derived from the natural products distamycin A and netropsin (11). Distamycin A is cytotoxic at relatively high concentrations (12), and inhibits the activity of RNA polymerase, DNA polymerase, topoisomerases I and II, and helicases (13-15). Previously, we showed that hairpin Py-Im polyamides designed to bind the androgen response element (ARE) decrease the expression of prostate cancer related genes, inhibit RNA polymerase activity, upregulate p53, and induce apoptosis (16,17). Curiously, no evidence of DNA breaks, which usually occurs upon treatment with DNA damaging agents such as doxorubicin, was observed. However, effects on replication remain to be investigated.

Here we report that hairpin Py-Im polyamides targeted to the ARE cause replication stress, resulting in an accumulation of S-phase cells. Furthermore, the polyamide-induced checkpoint response activates ATR and downstream phosphorylation of the mini-chromosome maintenance complex (MCMs), but not the downstream ATR effector kinase Chk1. The checkpoint response also results in monoubiquitination of the Fanconi anemia/Breast cancer (FA/BRCA) gateway protein FANCD2. The checkpoint is activated despite low levels of ssDNA formation and the absence of observable DNA breaks. We also show that polyamides are potent inhibitors of helicase unwinding *in vitro*, suggesting a model in which polyamides preclude fork progression through DNA-

binding. These results demonstrate that polyamides are capable of imposing replication stress and can activate both a non-canonical Chk1-independent ATR-checkpoint response and the FA/BRCA pathway, resulting in S-phase delay.

2.2 Results

Py-Im polyamides cause accumulation of S-phase cells and PCNA foci.

Hairpin Py-Im Polyamides **1** and **2** were designed to target the ARE (5'-GGTACANNNTGTTCT-3' (18)) and antagonize gene expression changes driven by the androgen receptor (AR) in the prostate cancer cell line, LNCaP (Figure 1A and B) (16,19). In LNCaP cells, AR signaling plays a critical role in cell proliferation (20), and therefore disruption of AR-dependent signaling may contribute to cell death. However, disruption of other DNA-dependent processes such as RNA pol II transcription elongation may also cause cell death. To investigate the effects of polyamides outside of AR-dependent transcription, we first compared the cytotoxicity of polyamides **1** and **2** in three different prostate cancer cell lines, LNCaP, LNAR, and DU145, which express high, normal, and low levels of AR, respectively. Polyamides **1** and **2** displayed dose-dependent cytotoxicity at 72 and 96 h as measured by sulfarhodamine B staining (Table 2.1). Polyamide **2** had approximately ten-fold higher potency than polyamide **1**, which is consistent with its greater potency against AR-driven gene expression (19). Importantly, the IC₅₀ values were similar in all cell lines regardless of AR status, suggesting that the observed cytotoxicity occurred via an AR-independent mechanism. In DU145 cells, expression of an AR-driven reporter is insensitive to androgen treatment and AR is

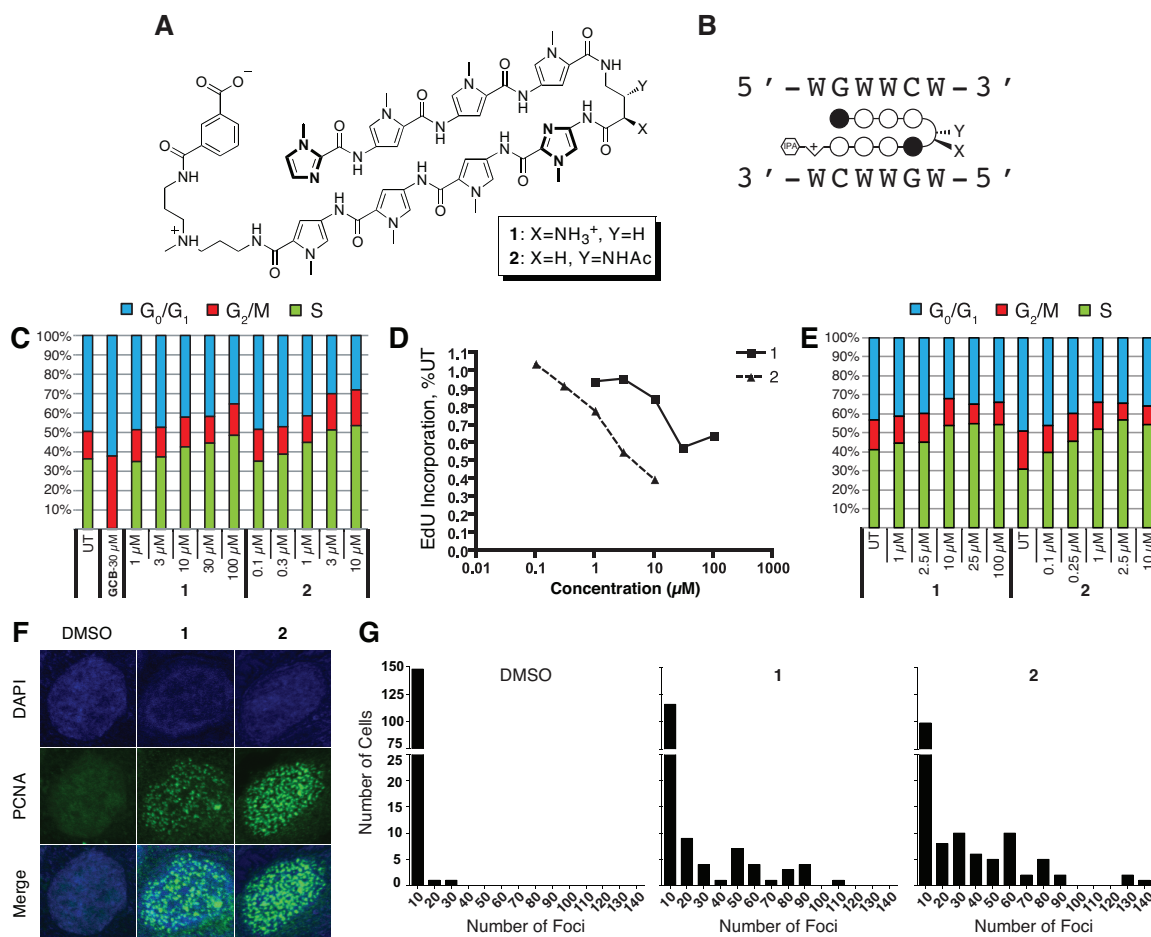


Figure 2.1 Polyamides cause accumulation of S-phase cells and PCNA foci. **(A)** Chemical structure Py-Im polyamides used in this study. **(B)** Ball-and-stick representation of the polyamides. Open circles represent N-methylpyrrole residues, filled circles represent N-methylimidazoles. The hexagon represents the isophthalic acid moiety. Polyamides **1** and **2** are specific for the same 5'-WGWWCW-3' DNA sequence, where W=A or T. **(C)** Cell cycle distribution of DU145 cells untreated (UT) or treated with gemcitabine (GCB), polyamide **1**, or polyamide **2** for 24 h as measured by two-color flow cytometric evaluation of EdU pulse-labeled cells stained for DNA content with 7AAD. **(D)** Dose-dependent decrease in average EdU incorporation indicative of slowed DNA synthesis in response to polyamide treatment. **(E)** Cell cycle distribution of DU145 cells untreated or treated with polyamide **1** or **2** for 48 h as measured by single-color flow cytometric evaluation of propidium iodide stained cells. **(F)** Representative images of immunofluorescent detection of PCNA in DU145 cells. Treatment with either 10 μM polyamide **1** or 1 μM **2** for 36 h causes more cells to contain significant punctate staining of PCNA. **(G)** PCNA foci counts for each cell are plotted in a histogram with bin sizes of 10 foci for each condition. 150 cells over three replicates were counted for each condition. Kruskal-Wallis test reports $P < 0.0001$ for **1** versus DMSO and **2** versus DMSO.

minimally expressed (21). Therefore, DU145 cells provide an environment to investigate the effects of polyamides **1** and **2** independent of AR-signaling.

Next, we examined the effects of polyamides **1** and **2** on the cell cycle in DU145 cells. We pulse-labeled exponentially growing and asynchronous DU145 cells with ethynyldeoxyuridine (EdU) after 24 h of polyamide treatment. Both polyamides produced a dose-dependent increase in the percentage of cells in S-phase, with a corresponding drop in the percentage of G0/G1 cells (Figure 1C). Although more cells were in S-phase, the average intensity of EdU staining decreased, suggesting that the treated cells were replicating their DNA more slowly and thus cells spent longer in S-phase (Figure 1D). Similar results were also obtained using traditional one-color flow cytometry to determine the cell cycle distribution after 48 h of polyamide treatment (Figure 1E).

We then determined whether replication/repair foci accumulated in the treated cells using PCNA immunofluorescence (22,23). We chose treatment conditions to allow for maximal effect on the cells before any significant decrease in viability or activation of

		Cytotoxicity IC ₅₀ values (μM)			
Cell line	AR	1		2	
		72h	96h	72h	96h
LNAR	+++	40±10	36±14	3±1	1.5±0.2
LNCaP	+	18±4	7±3	1.8±0.9	0.6±0.2
DU145	-	14±4	8±4	1.5±0.5	0.76±0.06

Table 2.1 Summary of cytotoxicity IC₅₀ values of polyamides **1** and **2** prostate cancer cell lines. Cell lines expressing different levels of AR were studied: AR-overexpressing (+++, LNAR), AR-expressing (+, LNCaP), and AR-negative (-, DU145) cancer cell lines. Cells were treated continuously with polyamides for 72 or 96 h before fixation and staining. Values represent the mean ± S.D. of three replicates.

apoptosis, as measured by mitochondrial reduction activity and caspase 3/7 activation (Figure 2.2). Nearly all DMSO treated cells showed 0-2 foci per cell, while polyamide treatment resulted in a significant increase in cells with greater than 20 foci (Figure 1F and G). Interestingly, some of the polyamide-treated cells but none of the DMSO-treated cells showed more than 50 foci. Observation of cells with such high incidence of foci suggests that polyamides cause prolonged stalling of replication forks and the recruitment of repair machinery (22).

Py-Im Polyamide treatment induces ATR activation.

S-phase accumulation subsequent to treatment with a DNA-binding compound was suggestive of checkpoint activation in response to replication stress. We therefore

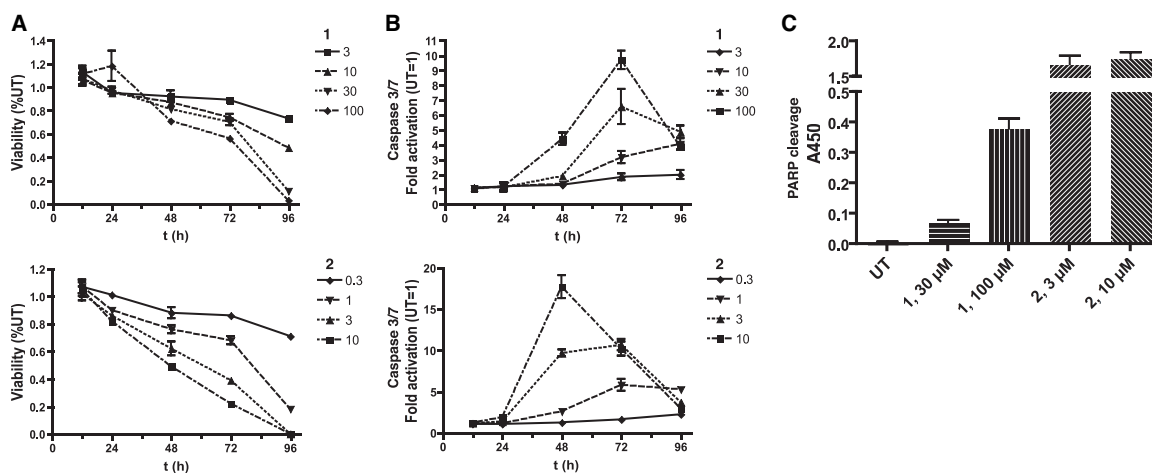


Figure 2.2 Polyamides induce apoptosis in DU145 cells. (A) Cell viability assay. Cells were treated in quadruplicate with polyamide 1 (top) or polyamide 2 (bottom) for range of concentrations (μM) for up to 96 h and then assayed for bioreductive capacity with WST-1 reagent. The data are normalized to the untreated condition. (B) Caspase 3/7 activity assay. Cells were treated in triplicate with polyamide 1 (top) or polyamide 2 (bottom) for the indicated time and then homogenized in guanidinium lysis buffer containing a pro-luminescent Caspase 3/7 substrate. The data are normalized to the untreated condition. (C) ELISA for cleaved PARP formation. Cells were treated with polyamides for 72 h. before assaying the lysates by sandwich ELISA using an HRP-conjugated secondary antibody and a chromogenic substrate. The data are presented as the background-corrected absorbance values at 450 nm. Error bars represent the mean ± S.D. of experiments conducted in triplicate or quadruplicate.

probed for activation of the master regulator kinases, ATR and ATM. We assayed ATR activation by immunoblotting for T1989 phosphorylation, an autophosphorylation site that has been implicated in ATR activation and a robust checkpoint response (24,25). Cells treated with polyamide **1** or **2** showed a slight increase in ATR T1989 phosphorylation relative to DMSO treated cells (Figure 2.3A). However, cells treated with hydroxyurea (HU), which causes nucleotide depletion, showed greater ATR T1989 phosphorylation compared to polyamide-treated cells suggesting a weaker activation of ATR by polyamides. NU6027, which inhibits cellular ATR but not ATM, did not abrogate T1989 phosphorylation under polyamide treatment (26). While polyamide treatment appeared to activate ATR, polyamides did not induce ATM S1981 phosphorylation, an autophosphorylation site that has been associated with ATM activation and stabilization at DSBs (Figure 2.3B) (27).

The weak phosphorylation of ATR suggested that polyamide treatment might result in limited ssDNA formation (4). To directly probe for ssDNA accumulation, we preincubated cells with the thymidine analog, 5-chloro-2'-deoxyuridine (CldU), and then treated with polyamide or HU. After treatment, we fixed the cells and immunostained using an anti-CldU antibody, which reacts with CldU exposed in ssDNA but not dsDNA. About 25% of cells on average showed >10 CldU foci after treatment with HU, while only about 3% and 1% of cells showed >10 CldU foci after 12 h treatment with high concentrations of polyamide **1** or **2** (Figure 2.3C and D). When treated with lower concentrations of polyamide **1** or **2** for 36 h post-CldU incubation, about 8% and 9% cells were positive for CldU foci. However, among the positive cells present under polyamide

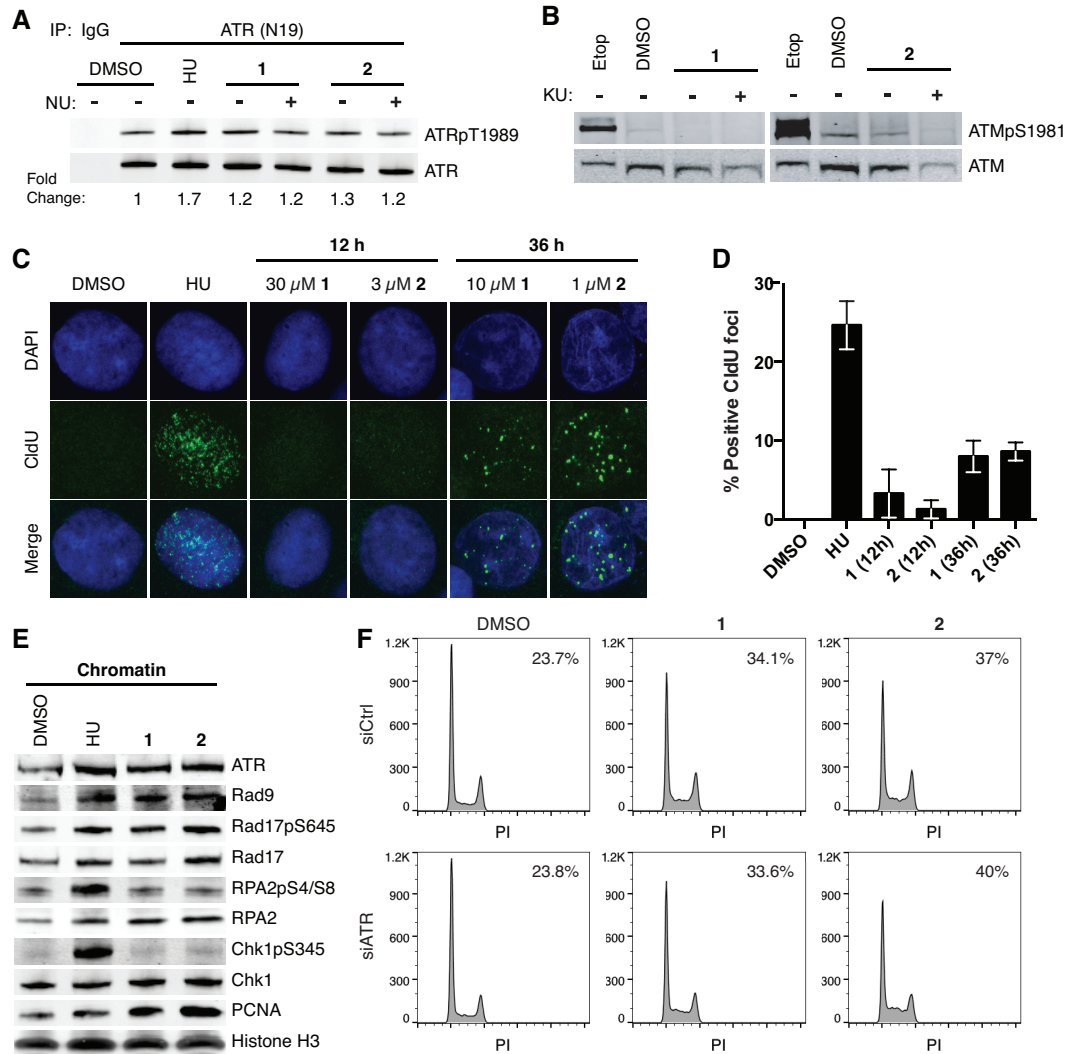


Figure 2.3 Polyamides induce ATR activation without extensive ssDNA formation. **(A)** Immunoblot of ATRpT1989 and ATR following IP of ATR in DU145 whole cell lysates treated with 4 mM hydroxyurea (HU) for 2 h, and DMSO, 10 μ M polyamide **1**, or 1 μ M polyamide **2** in the presence or absence of 10 μ M NU6027 (NU, ATR inhibitor) for 36 h. **(B)** Immunoblots of ATMpS1981 and ATM after treatment with 30 μ M etoposide (Etop) for 30 min, and DMSO, 10 μ M polyamide **1**, or 1 μ M polyamide **2** in the presence or absence of 10 μ M KU55933 (KU, ATM inhibitor) for 36 h. **(C)** Representative images of ssDNA formation via CldU immunofluorescence under non-denaturing conditions are shown for cells after treatment with 4 mM HU for 2 h, DMSO, 30 μ M polyamide **1**, or 3 μ M polyamide **2** for 12 h, and 10 μ M polyamide **1** or 1 μ M polyamide **2** for 36 h. **(D)** Bar graphs of the mean and standard deviation of percent CldU positive cells (>10 foci/cell). 150 cells over three replicates were counted for each condition. **(E)** Immunoblots of ATR and checkpoint related factors loaded onto chromatin upon treatment with 10 mM HU for 2 h, and DMSO, 10 μ M polyamide **1**, or 1 μ M polyamide **2** for 36 h. **(F)** DNA histograms of propidium iodide (PI) stained DU145 cells after treatment with negative control or ATR-targeting siRNA for 48 h followed by treatment with DMSO, 10 μ M polyamide **1**, or 1 μ M polyamide **2** for 36 h. The percentage of cells in S-phase is included at the top right of each graph.

treatment the number of CldU foci was substantially lower than in HU treated cells. Thus, the degree of ssDNA formation in polyamide treated cells was also lower than in HU treated cells, consistent with the lower levels of T1989 phosphorylation observed.

To confirm ATR activation, we determined if ATR and mediators of the ATR response accumulate on chromatin after polyamide treatment. Polyamide treatment resulted in ATR loading onto chromatin (Figure 2.3E). Interestingly, although we had observed a lower level of ATR phosphorylation in polyamide treated cells than in HU treated cells (Figure 2.3A), similar amounts of ATR were loaded onto chromatin following each treatment. Polyamide treatment also induced loading of RPA, the Rad9-Rad1-Hus1 (9-1-1) complex, which is integral to ATR checkpoint signaling, and Rad17, which is part of the clamp loader that facilitates 9-1-1 loading, to similar levels as did HU. Rad17 S645, a target for ATR phosphorylation that is necessary for G2 checkpoint activation (28), was phosphorylated in the presence of polyamide, indicating that ATR was activated. Polyamide treatment also induced higher PCNA loading on chromatin, which is consistent with the high incidence of PCNA foci formation (Figure 2.1D). Despite the lack of extensive ssDNA formation, ATR as well as its mediators are recruited to chromatin and ATR is active after polyamide treatment.

Py-Im Polyamide-induced S-phase delay is not abrogated by ATR knockdown.

To determine whether the activation of ATR had physiological consequences, we monitored the effect of siRNA knockdown of ATR on accumulation of polyamide treated cells in S-phase. The percentage of S-phase cells was the same in cells treated with either

siRNA against ATR or negative control siRNA prior to treatment with polyamide **1** or **2** (Figure 2.3F). This suggests that ATR activity is not contributing to S-phase accumulation. When caffeine, a PI3 kinase inhibitor with preference for ATR over ATM, was added to cells in addition to polyamide **1** or **2**, the S-phase population was reduced compared to cells treated only with polyamide; however, caffeine treatment also reduces the basal level of S-phase cells and may account for this decrease (Figure 2.4). Similarly, when the ATR inhibitor NU6027 was added to cells the S-phase population was reduced under both the basal and polyamide-treated conditions.

Although ATM S1981 was not phosphorylated in response to polyamide treatment, ATM autophosphorylation sites other than S1981 have been implicated in its activation and function in the cell cycle checkpoint (29). Therefore the effects of ATM inhibition were also monitored. KU55933, a selective inhibitor of ATM, did not diminish the polyamide induced S-phase accumulation (Figure 2.4) (30).

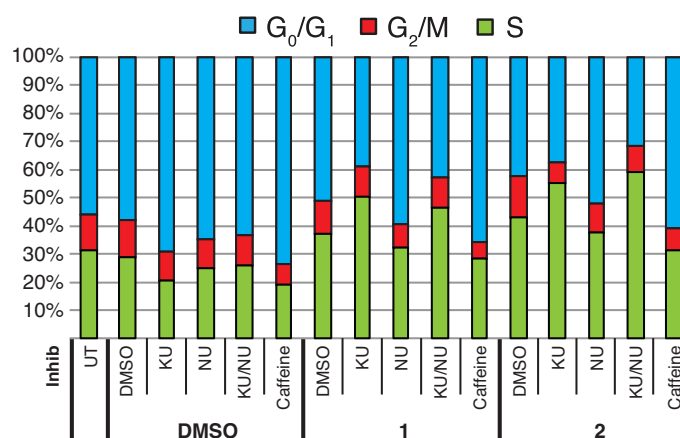


Figure 2.4 Effects of small molecule PI3-kinase inhibitors on polyamide-induced S-phase accumulation. Cell cycle distribution of DU145 cells after 36 h treatment with DMSO, 10 μ M polyamide **1**, or 1 μ M polyamide **2** in the presence of 2 mM caffeine, 10 μ M KU55933 (KU, ATM inhibitor), or 10 μ M NU6027 (NU, ATR inhibitor) as measured by single-color flow cytometric evaluation of propidium iodide stained cells. When both KU and NU were added together with DMSO or polyamide, only 4 μ M of each inhibitor was used to reduce toxicity.

Py-Im Polyamide treatment does not induce Chk1, RPA2, or Chk2 phosphorylation.

The ATR-mediated checkpoint response can be propagated by a variety of downstream effectors. Chk1, the best studied of the ATR effectors, signals cell cycle delay after activation by ATR via phosphorylation at S345. Surprisingly, Chk1 S345 was not phosphorylated after treatment with polyamide (Figure 2.3E). Chk1 S345 phosphorylation is dependent upon RPA2 hyperphosphorylation at sites S4 and S8, which occurs following DSBs from collapsed replication forks (31). Polyamide treatment also did not induce phosphorylation of RPA2 S4/S8. To ensure that we were not missing a transient activation of Chk1 or RPA2, we assayed for their phosphorylation across multiple time points. In addition, we monitored other known Chk1 and RPA2 phosphorylation sites including Chk1 S317 and S296 and RPA2 S33. Chk1 S317 is another target for phosphorylation by ATR in response to replication stress, and Chk1 S296 is an autophosphorylation site that is important for its function (32). RPA2 S33 phosphorylation by ATR under replication stress protects cells by stimulating DNA synthesis and facilitates S4/S8 phosphorylation by DNA-PKcs (31,33). After 12, 18, 36, and 72 h of treatment with polyamide **1** or **2** neither Chk1 nor RPA2 were phosphorylated at any of the sites monitored (A). To test the possibility that polyamide **1** and **2** may somehow inhibit ATR from phosphorylating Chk1, DU145 cells were treated with both polyamide **1** or **2** and aphidicolin, a DNA polymerase inhibitor that induces Chk1 S345 phosphorylation. The polyamides did not inhibit aphidicolin-induced Chk1 S345 phosphorylation (Figure 2.5A and B).

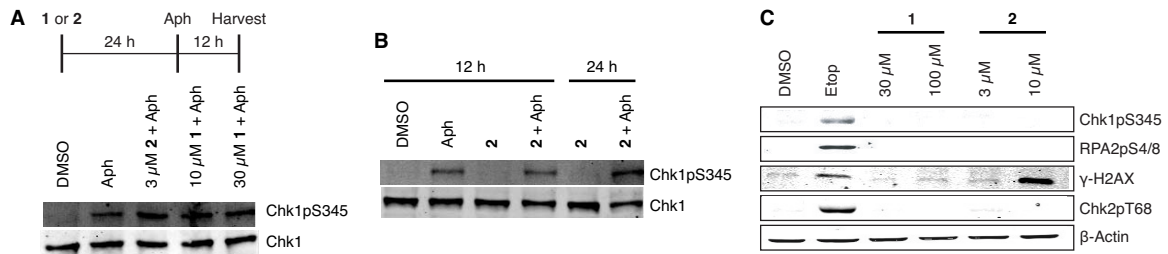


Figure 2.5 High concentration polyamide treatment does not inhibit aphidicolin-induced Chk1 phosphorylation. (A) Immunoblot of Chk1pS345 after the treatment with polyamides followed by aphidicolin. DU145 cells were treated with DMSO, 10 μM polyamide 1, or 1 μM polyamide 2 followed by the addition of 10 μg/mL aphidicolin (Aph) after 24 h. Cells were harvested after 36 h total incubation. (B) Immunoblot of Chk1pS345 after simultaneous treatment of DMSO or 3 μM polyamide 2 plus 10 μg/mL aph for 12 or 24 h. (C) Immunoblot of S-phase checkpoint and DNA damage response proteins, Chk1pS345, RPA2pS4/8, Chk2pT68, and γ-H2AX in DU145 cells after 18 h treatment with DMSO, 30 μM etoposide, polyamide 1, or polyamide 2 at the indicated concentrations.

The absence of Chk1 or RPA2 phosphorylation led us to investigate phosphorylation of Chk2, another cell cycle checkpoint kinase, and H2AX, a histone variant that is phosphorylated rapidly upon DNA damage, as possible downstream checkpoint mediators. ATM predominantly phosphorylates Chk2 T68, though there is evidence for phosphorylation of Chk2 by ATR following cisplatin treatment (34,35). Similarly, ATM or ATR can phosphorylate H2AX S139 in response to different types of replication stress (36). Consistent with the absence of ATM S1981 phosphorylation after polyamide treatment, polyamides failed to induce Chk2 T68 phosphorylation (Figure 2.6A). H2AX and RPA2 S4/S8 phosphorylation were slightly elevated after 72 h treatment of 1 μM polyamide 2, and may be suggestive of DNA damage. However, H2AX can be phosphorylated under non-damaging stress (37). It is also worth noting that these phosphorylation events may be triggered by apoptosis, which occurs after 72 h treatment with polyamide 2 (Figure 2.2). Finally, we also studied the effect of high

concentration polyamide treatment for 18 h and similar results were observed (Figure 2.5C).

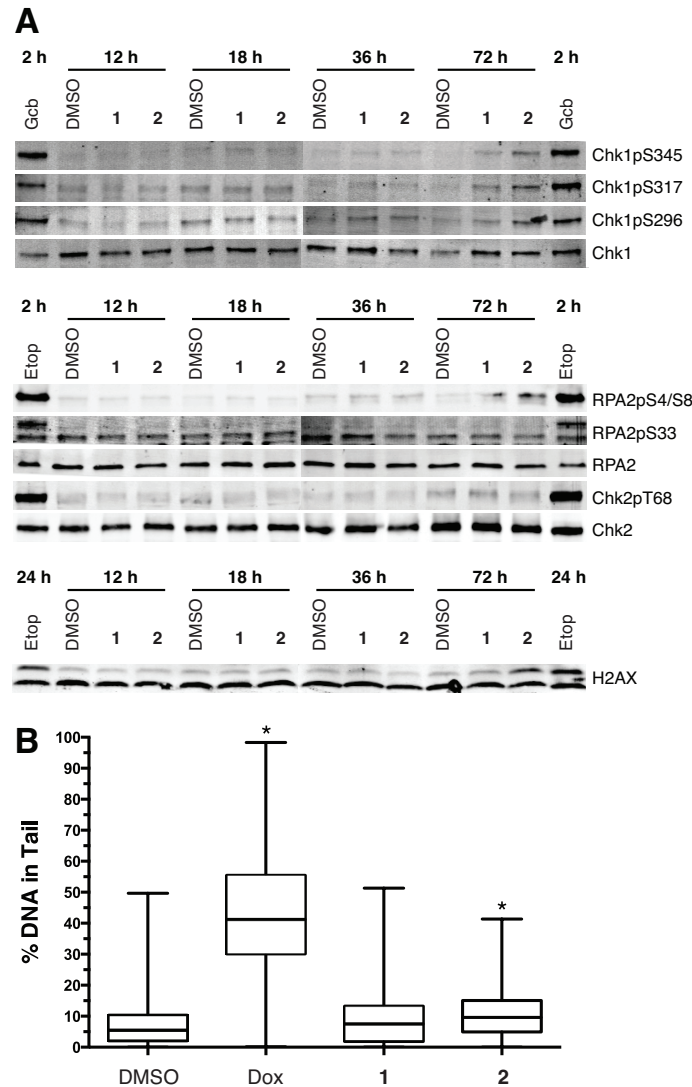


Figure 2.6 Polyamides do not induce phosphorylation of Chk1, RPA2, or Chk2 or observable DNA breaks. (A) Immunoblots of phosphorylated Chk1 at S345, S317, and S296; RPA2 S4/S8 and S33; Chk2 T68; and H2AX S139 after 12, 18, 36, and 72 h treatment with DMSO, 10 μ M polyamide 1, 1 μ M polyamide 2, or treatment with 30 μ M gemcitabine (Gcb) for 2 h or 30 μ M etoposide (Etop) for 2 h and 24 h in whole cell lysates. (B) Single cell alkaline gel electrophoretic analysis DU145 cells treated with 1 μ M doxorubicin (Dox) for 24 h, and DMSO, 10 μ M polyamide 1, or 1 μ M polyamide 2 for 36 h. Boxes show the median percentage of DNA in the comet tail and are bounded by 25th and 75th percentile while whiskers represent the min and max percentile. 400 cells from two biological replicates were counted for each condition. Mann Whitney test reports $P < 0.0001$ for Dox and 2, and is indicated by *.

Py-Im polyamide treatment does not induce DNA breakage.

The absence of ATM, Chk2, and RPA2 phosphorylation suggested that polyamide-induced replication stress does not lead to gross breakage of DNA. To study DNA breakage directly, we treated cells with polyamides and then analyzed them by single cell alkaline gel electrophoresis (Figure 2.6B). Migration of the DNA from the centroid into the ‘comet tail’ is proportional to the amount of single- and double-strand breakage that has occurred. Cells treated with doxorubicin, a known DNA-damaging agent, were used as a positive control and showed a median value of 41% of total DNA in the tail. Polyamide-treated cells, however, were similar to the DMSO control with median %DNA in tail values of 8 and 10 for polyamides **1** and **2**, respectively, compared to 6% for DMSO. The lack of extensive DNA breakage correlates with the absence of ATM-Chk2 activation.

Py-Im Polyamide treatment induces MCM2 phosphorylation and monoubiquitination of FANCD2, a major gatekeeper of the FA/BRCA Repair Pathway.

Since Chk1, Chk2, and RPA2 were not phosphorylated, our results suggested that ATR phosphorylates targets intrinsic to the replication fork to regulate S-phase progression. MCM2 is a component of the replicative helicase and is required for both initiation and elongation phases of DNA replication. MCM2 S108 is phosphorylated by ATR and ATM in response to stalled replication and DSBs (38). This phosphorylation is thought to be an attempt by the cells to promote the firing of local dormant replication origins via Plk1 in order to ensure complete replication (39). We monitored MCM2 phosphorylation for response to polyamide-induced replication stress. Treatment with

polyamide **1** or **2** resulted in a time-dependent increase of MCM2 S108 phosphorylation (Figure 2.7A). The level of MCM2 phosphorylation observed after 36 h polyamide treatment was similar to that observed after 2 h HU treatment. Polyamide-induced

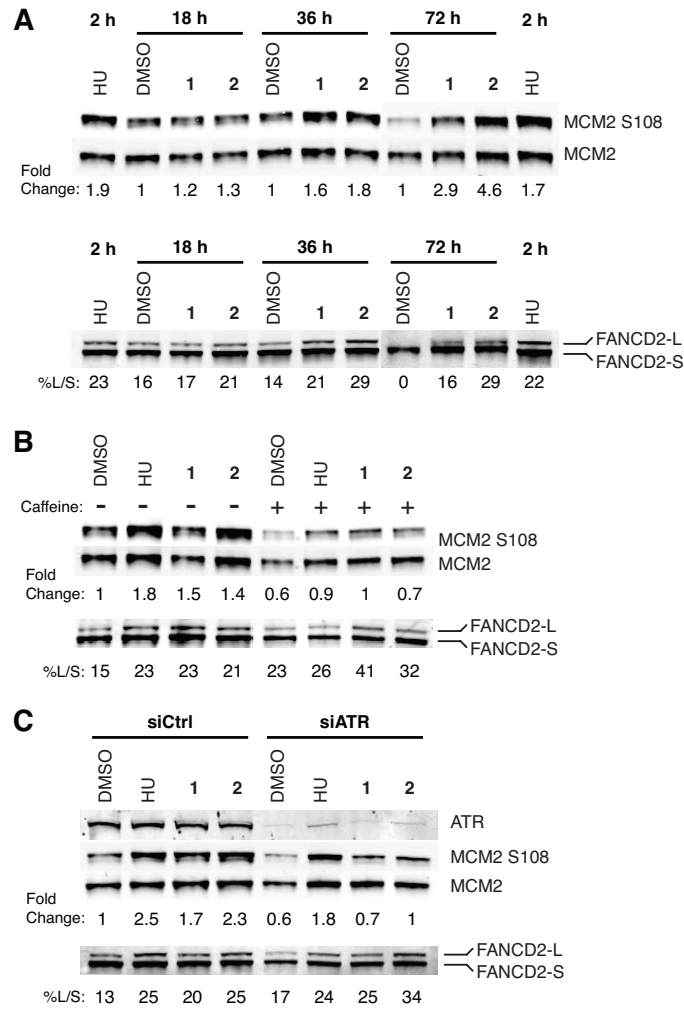


Figure 2.7 Polyamides induce phosphorylation of MCM2 and FANCD2 monoubiquitination. **(A)** MCM2 S108 phosphorylation and FANCD2 monoubiquitination levels were measured in DU145 cells treated with 4 mM HU for 2 h, and DMSO, 10 μ M polyamide **1** or 1 μ M polyamide **2** over a time course of 18, 36, and 72 h. Monoubiquitination was estimated by normalizing the band intensity of the large molecular weight monoubiquitinated FANCD2 band (FANCD2-L) to the low molecular weight non-ubiquitinated FANCD2 band (FANCD2-S). **(B)** MCM2 S108 phosphorylation and FANCD2-Ub levels were measured in cells treated with 4 mM HU for 2 h, and DMSO, 10 μ M polyamide **1** or 1 μ M polyamide **2** for 36 h with or without the addition of 2 mM caffeine. **(C)** MCM2 S108 phosphorylation and FANCD2-Ub levels were measured in cells treated with negative control or ATR-targeting siRNA for 48 h prior to the addition of 4 mM HU for 2 h, and DMSO, 10 μ M polyamide **1** or 1 μ M polyamide **2** for 36 h.

MCM2 S108 phosphorylation was also inhibited by co-treatment with caffeine (Figure 2.7B). To determine the contribution of ATR to MCM2 phosphorylation, ATR was knocked down using siRNA prior to polyamide treatment, and similar levels of inhibition were observed as under caffeine treatment (Figure 2.7C). We also investigated the contributions of ATR and ATM to MCM2 phosphorylation using the small molecule kinase inhibitors NU6027 and KU55933. Both inhibitors reduced MCM2 phosphorylation levels induced by HU or polyamide, with a stronger effect from NU6027 (Figure 2.8A). Together, these observations suggest that ATR is the predominant mediator of polyamide-induced MCM2 phosphorylation.

Recently, the FA/BRCA pathway protein FANCD2 was implicated in a general replisome surveillance mechanism (40). In response to replication stress, FANCD2 undergoes ATR-dependent monoubiquitination (41), which is critical for prolonged localization to chromatin at stalled replication forks (40,42). FANCD2 functions to protect stalled forks from degradation (42) and physically interacts with phosphorylated MCM2 (40), though interaction with MCM2 is not dependent upon monoubiquitination. This led us to search for polyamide-induced monoubiquitination of FANCD2 as a marker of FA/BRCA pathway activation. Treatment with polyamide **1** or **2** caused a time-dependent increase in monoubiquitinated FANCD2 (FANCD2-Ub) (Figure 2.7A). FANCD2-Ub was present in vehicle treated samples, which is perhaps a consequence of DU145 cells' endogenous genomic instability. Surprisingly, inhibition of ATR through the use of caffeine or siRNA both failed to decrease the level of polyamide-induced FANCD2-Ub (Figure 2.7B and C). In addition, the ATR inhibitor NU6027 increased the

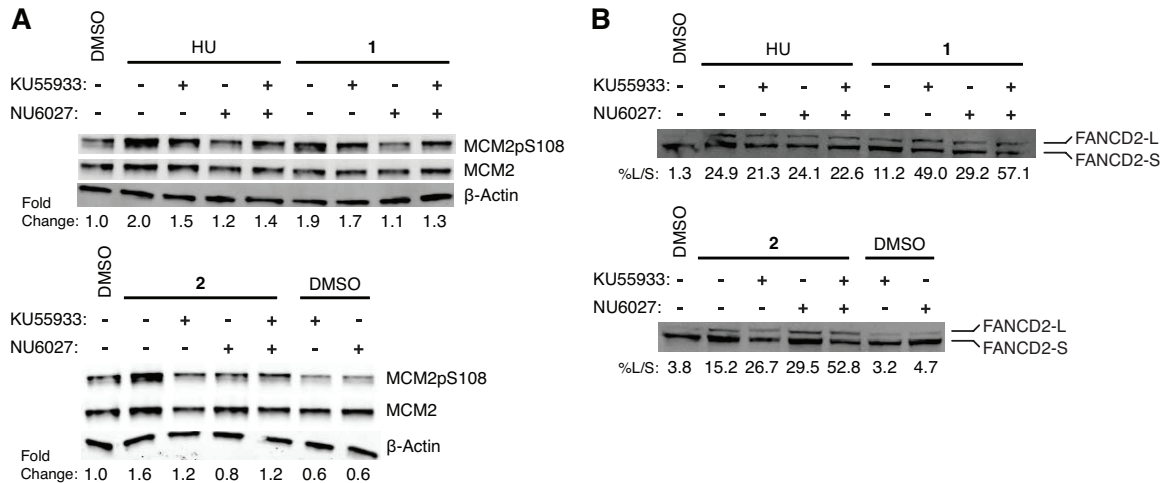


Figure 2.8 Effects of ATM- and ATR-specific small molecule inhibitors on polyamide-induced MCM2 S108 phosphorylation and FANCD2 monoubiquitination. **(A)** MCM2 S108 phosphorylation levels were measured in DU145 cells treated with 4 mM HU for 2 h, and DMSO, 10 μ M polyamide **1** or 1 μ M polyamide **2** for 36 h in addition to 10 μ M KU55933 (KU, ATM inhibitor), 10 μ M NU6027 (NU, ATR inhibitor), or both KU and NU. Only 4 μ M KU and 4 μ M NU were used when both inhibitors were added together to reduce toxicity. **(B)** FANCD2-Ub levels were measured in selective kinase inhibitor-containing lysates. Monoubiquitination was estimated by normalizing the band intensity of the large molecular weight monoubiquitinated FANCD2 band (FANCD2-L) to the low molecular weight non-ubiquitinated FANCD2 band (FANCD2-S).

fraction of FANCD2-Ub in response to polyamide treatment (Figure 2.8B). These results may be unique to DU145 cells, as ATR knockdown by siRNA has been shown to abrogate FANCD2 ubiquitination in the presence of high levels of replication fork damage caused by 12 h treatment of HU or mitomycin C (MMC) in U2OS cells (43). The ATM inhibitor KU55933 similarly increased FANCD2-Ub levels when co-treated with polyamides, though this result is consistent with previous studies (Figure 2.8B) (44).

Next, we confirmed the functional role of FANCD2 in resisting the toxic effects of polyamides in a model outside of prostate cancer. The FANCD2 deficient fibroblast cell line PD20 complemented with an empty vector exhibited greater sensitivity to

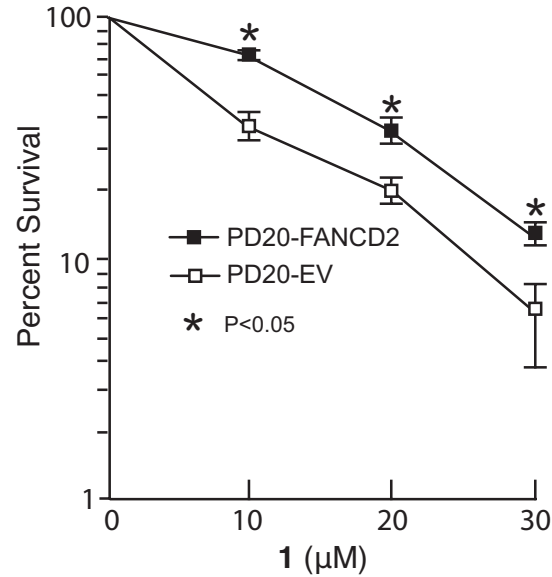


Figure 2.9 FANCD2 increases cell survival after exposure to polyamide **1**. PD20 cells complemented with empty vector (PD20-EV) or FANCD2 (PD20-FANCD2) were treated with the indicated concentrations of polyamide **1** for 36h and assayed for survival after 14 days. Error bars indicate mean \pm SEM for n=3 independent experiments. Unpaired T-tests were performed at *P<0.05.

polyamide treatment than PD20 cells complemented with a FANCD2-expressing vector (Figure 2.9). Together, these data support the conclusion that MCM2 and FANCD2 participate in the response to polyamide-induced replication stress in addition to ATR.

We also tested whether FANCD2 participated in the S-phase accumulation observed in response to polyamide treatment. Similar to Figure 2.3F, we tested whether knockdown of FANCD2 by siRNA prior to the addition of polyamides **1** or **2** would prevent cells from accumulating in S-phase (Figure 2.10). Knockdown of FANCD2 did not prevent cells from accumulating in S-phase, therefore suggesting that its role in the stress response is not necessarily to activate the intra-S-phase checkpoint to prevent cells from entering G2.

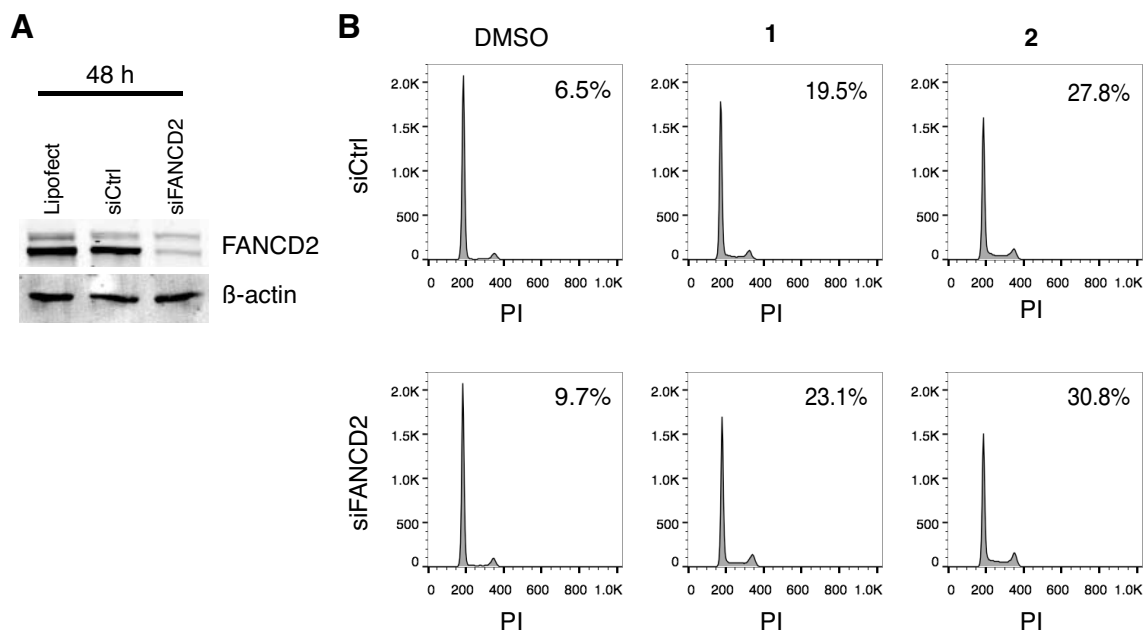


Figure 2.10 Knockdown of FANCD2 by siRNA does not prevent the accumulation of DU145 cells in S-phase in response to polyamide treatment. **(A)** Immunoblot depicting the knockdown of FANCD2 by treatment with 25 nM siRNA for 48 h. **(B)** DNA histograms of propidium iodide (PI) stained DU145 cells after treatment with negative control or ATR-targeting siRNA for 48 h followed by treatment with DMSO, 10 μ M polyamide **1**, or 1 μ M polyamide **2** for 36 h. The percentage of cells in S-phase is included at the top right of each graph.

Polyamide 1 inhibits T7 gp4A helicase activities in vitro.

The results from cell culture experiments suggested a model in which polyamides stall replication forks without causing extensive ssDNA or DNA breaks and that the ATR and the FA/BRCA pathways are activated. The high affinity DNA-binding properties of polyamides coupled with limited ssDNA formation suggested that polyamides might inhibit unwinding of the replication fork. To test this hypothesis, we determined the ability of polyamide **1** to inhibit DNA helicases *in vitro*. We first studied a strong replicative, hexameric helicase similar to the MCM2-7 complex. Testing both polyamides was deemed unnecessary for this particular study, as both polyamides **1** and **2** have comparable binding affinities *in vitro*, as shown by a duplex DNA thermal stabilization assay (Figure 2.11). We used T7 gp4A, the well-studied T7 phage homohexameric

replicative helicase (45). We followed unwinding of a forked duplex DNA substrate containing either a single match site or no match sites for polyamide **1** by gel electrophoresis (45). Helicase inhibition was measured by the percent of unwound substrate relative to the mock treated sample. Incubating polyamide **1** with the substrate containing the match site resulted in effective inhibition of gp4A helicase activity ($IC_{50} \sim 5\text{nM}$) (Figure 2.12A, top). The polyamide was still able to inhibit gp4A helicase activity on the mismatch substrate but required significantly higher concentrations of polyamide ($IC_{50} \sim 335\text{ nM}$), owing to the sequence specificity of polyamides (Figure 2.12A, bottom). Similar results were also obtained when using a different class of helicase, *S. cerevisiae* Dna2 (Figure 2.13). These results suggest that the polyamide is not directly interacting with the helicases but acts through DNA binding.

The sequence specific non-covalent binding nature of polyamides led us to hypothesize that helicase inhibition would not only be stronger at a given concentration when comparing the match to the mismatch substrate but that the enzyme would also show slower unwinding kinetics given the polyamide's longer dwell time at a match site.

A			B			C		
5' -TCGC AGAACA GCGA-3'			5' -GT AGAACA GCGACC-3'			5' -C AGAACA GCAGTCG-3'		
3' -AGCG TCTTGT CGCT-5'			3' -CA TCTTGT CGCTGG-5'			3' -G TCTTGT CGTCAGC-5'		
$T_m = 61.7 (\pm 0.4) ^\circ\text{C}$			$T_m = 61.4 (\pm 0.3) ^\circ\text{C}$			$T_m = 61.3 (\pm 0.5) ^\circ\text{C}$		
	$T_m (^{\circ}\text{C})$	$\Delta T_m (^{\circ}\text{C})$		$T_m (^{\circ}\text{C})$	$\Delta T_m (^{\circ}\text{C})$		$T_m (^{\circ}\text{C})$	$\Delta T_m (^{\circ}\text{C})$
1	76.7 (± 0.1)	14.9	1	74.8 (± 0.1)	13.3	1	73.5 (± 0.4)	12.1
2	76.2 (± 0.2)	14.4	2	74.4 (± 0.2)	12.9	2	74.2 (± 0.3)	12.8

Figure 2.11 Py-Im Polyamides stabilize duplex DNA regardless of match site position in the duplex. DMSO or 4 μM polyamide was incubated with 2 μM 14 bp duplex DNA containing only a single 5'-WGWWCW-3' binding site positioned either 4 bps (A), 2 bps (B), or 1 bp (C) from the edge and a melting curve was measured using DNA hyperchromicity (46). The average melting temperature and standard deviation were calculated from four replicates.

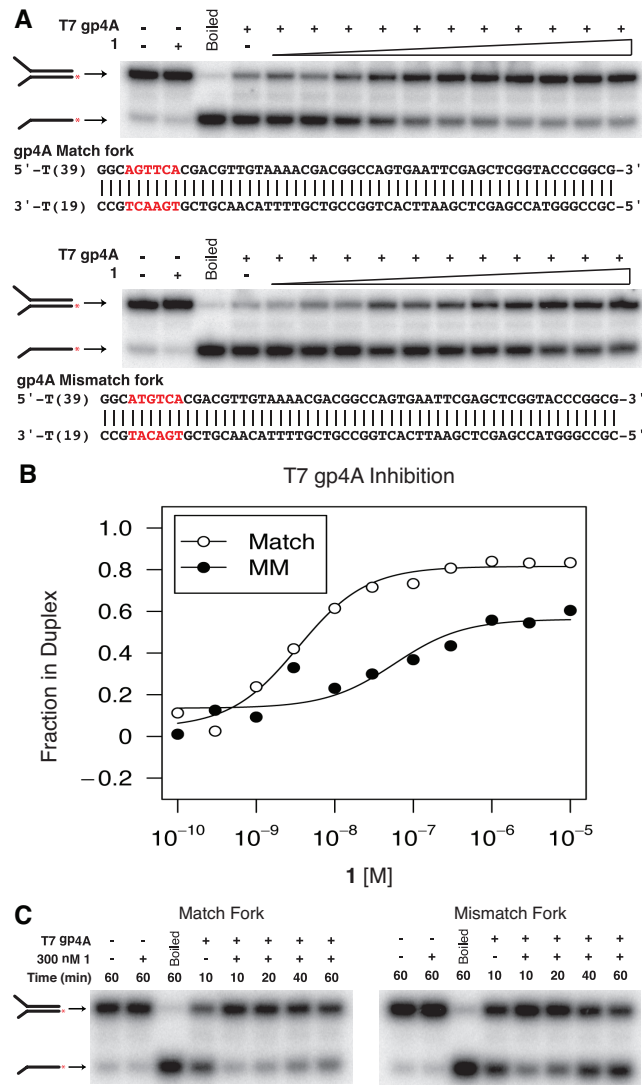


Figure 2.12 Polyamide **1** inhibits T7 gp4A helicase activity. (A) Inhibition of T7 gp4A by polyamide **1** was tested using a forked DNA duplex containing a single match-binding site (top) or no match-binding site (bottom). ^{32}P is represented in the cartoon by the red asterisk. Polyamide **1** was added in increasing concentrations (lanes 4-15): 100 pM, 300 pM, 1 nM, 3 nM, 10 nM, 30 nM, 100 nM, 300 nM, 1 μM , 3 μM , 10 μM . (B) Graphical representation of gp4A inhibition curves. (C) Inhibition of gp4A was then assessed in the time domain by incubating the helicase reactions for increasing amounts of time with either the (left) matched or (right) mismatched substrate.

When using the match substrate, gp4A was unable to unwind as much substrate in the presence of polyamide as the mock treated sample even when allowed to incubate for longer times (Figure 2.12C, left). However, gp4A was capable of unwinding the same amount of mismatch substrate in the presence of polyamide as the mock treated sample

when allowed to incubate longer (Figure 2.12C, right). These data support helicase inhibition as one explanation for how polyamides cause replication stress.

2.3 Discussion

In the present study we determine that hairpin Py-Im polyamides designed to target the AR:DNA interface are cytotoxic and cause replication stress in androgen-insensitive DU145 cells. Polyamide-induced replication stress causes the accumulation of S-phase cells and PCNA foci, decreased replication, and triggers chromatin loading and activation of ATR. The ssDNA-binding protein subunit, RPA2, and the downstream effector kinase, Chk1, were not phosphorylated in response to polyamide treatment, even at high concentrations and after long incubations. ATR did, however, phosphorylate the MCM helicase subunit, MCM2. In addition, the phospho-MCM2 binding partner and FA/BRCA family member, FANCD2, was monoubiquitinated following polyamide treatment. ATR activation also led to phosphorylation of Rad17, the major subunit of the checkpoint clamp loader. In sum, the polyamide-induced checkpoint response, like that induced by nucleotide depletion, requires the general replisome surveillance pathway involving FANCD2, but does not also require the canonical Chk1 pathway that nucleotide depletion activates to mitigate the stress. Consistent with the DNA helix altering and duplex stabilization properties of polyamides, we showed that polyamides inhibit a hexameric replicative helicase *in vitro* and postulate a model in which non-covalently binding polyamides intermittently preclude replisome progression, resulting in a limited ATR checkpoint response (Figure 2.14A).

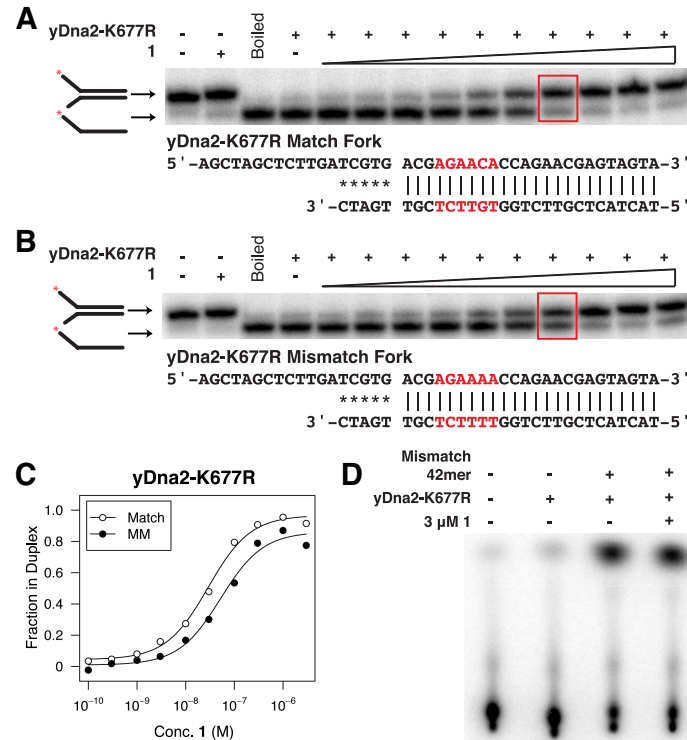


Figure 2.13 Polyamide **1** inhibits helicase activity of *S. cerevisiae* Dna2 nuclease dead but helicase active mutant (yDna2-K677R). Inhibition of yDna2-K677R by polyamide **1** was tested using a forked DNA duplex containing either one match-binding site (**A**) or no match-binding site (**B**). 32 P is represented in the cartoon of the substrate by the red asterisk. Polyamide **1** was added in increasing concentrations (lanes 4-14): 100 pM, 300 pM, 1 nM, 3 nM, 10 nM, 30 nM, 100 nM, 300 nM, 1 μ M, 3 μ M. (**C**) Graphical representation of yDna2-K677R inhibition curves. (**D**) 3 μ M polyamide **1** was incubated with the single-stranded mismatch DNA oligomer and yDna2-K677R to assess whether polyamide **1** can inhibit yDna2-K677R ATPase activity.

When activated at a stalled replication fork, ATR is critical for protection of the forks from collapse. ATR also suppresses the firing of dormant origins globally, presumably to prevent further replication-associated damage (6). Recently, Koundrioukoff *et al.* (47) reported that ATR could be activated in discrete stages. Low concentration aphidicolin treatment, which resulted in moderately reduced fork speeds, led to recruitment of ATR and ATR activators to chromatin as well as delayed mitotic entry but did not result in ssDNA accumulation or Chk1 phosphorylation. In addition, low concentrations of aphidicolin did not induce ATM or H2AX phosphorylation. Based

on the similarity in checkpoint response to polyamides, we propose that polyamides induce low level replication stress leading to ATR recruitment and cell cycle delay decoupled from Chk1 activity.

Although the previous work established that activation of the ATR checkpoint response might occur in the absence of downstream Chk1 activation, it did not identify the mediators of fork protection. Our findings implicate ATR-dependent phosphorylation of MCM2 and FA/BRCA pathway activation, as evidenced by monoubiquitination of FANCD2. ATR-mediated MCM2 phosphorylation has previously been shown to recruit Plk1 to stalled forks, which may allow origin firing near the stall for completion of replication (39). FANCD2 has been shown to bind nascent DNA at sites of replication stalling due to nucleotide depletion and, importantly, restrains replisome progression to minimize ssDNA accumulation (40,48). FANCD2 bound to nascent DNA interacts transiently but directly with the MCMs, including phosphorylated MCM2, though this interaction does not depend on monoubiquitination of FANCD2 (40). However, this interaction was shown to depend on ATR activity. It is interesting that polyamide-induced FANCD2 monoubiquitination in DU145 cells was not inhibited upon knockdown of ATR. The current model of FA/BRCA pathway activation, based on studies in U2OS osteosarcoma cells, DT40 chicken B cells, and *in vitro* assays, links ATR to downstream FANCD2 monoubiquitination through the phosphorylation of FANCI, a FANCD2 paralog, in the presence of catastrophic interstrand crosslinking damage or long term treatment with HU (41,43,49). It is possible that replication stress may trigger FANCI phosphorylation by a kinase other than ATR in DU145 cells, or that

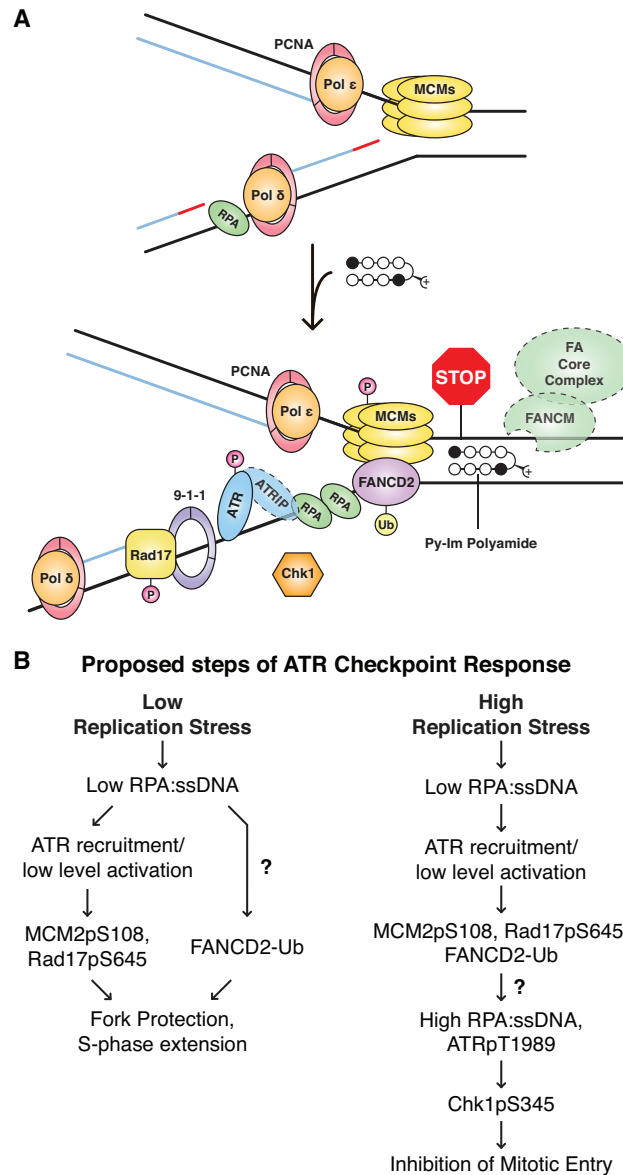


Figure 2.14 Putative model of Py-Im polyamide-induced replication stress and subsequent ATR-dependent checkpoint response. **(A)** Polyamides bind transiently at match sites throughout the genome, distorting the structure of the helix locally and precluding the progression of the replisome when encountering a fork. Stalled replication fork components that were not investigated directly (except polymerases) are outlined in dashed lines. **(B)** Proposed steps of ATR checkpoint response under low replication stress, such as polyamide treatment, or high replication stress, such as high concentration HU treatment. Our data supports the model for stepwise activation of ATR. First, ATR is recruited to chromatin and moderately phosphorylated, leading to MCM2 phosphorylation and Rad17 phosphorylation. FANCD2 is also monoubiquitinated and recruited to chromatin for fork protection. Then, if the stress is sufficiently high, such that replication forks are persistently stalled, ssDNA accumulation and higher ATR T1989 phosphorylation occur, followed by downstream phosphorylation of Chk1 by ATR. What triggers the switch leading to ssDNA accumulation and ATR-Chk1 activation is unclear.

FANCI is an ATR substrate under more severe forms of replication stress. However the FA/BRCA pathway is activated, our results suggest that the FA/BRCA pathway acts in concert with ATR-MCM2 signaling to stabilize replication forks in response to polyamide treatment. The lack of ATR-dependence on polyamide-induced S-phase accumulation is also notable, but consistent with published studies in U2OS cells treated with HU (43). Investigating the effects of knockdown of FA family genes on ssDNA formation and cell cycle phase distribution in polyamide-treated cells would be of interest for future studies.

In order to understand how ATR-MCM2 and FA/BRCA activation is related to ATR-Chk1 activation, we compared the checkpoint response induced by low replication stress, such as polyamide treatment, and high replication stress, such as high concentration HU treatment (Figure 2.15). Both treatments result in MCM2 phosphorylation and FANCD2 monoubiquitination (Figure 2.7), as well as recruitment of equivalent amounts of ATR and its mediators to chromatin (Figure 2.3E). However, polyamide treatment resulted in significantly lower levels of ssDNA formation (Figure 2.3C and D). Our data suggest that polyamide treatment either induces sufficient ssDNA for ATR recruitment, or perhaps triggers an alternative or cooperative mechanism to recruit ATR-ATRIP to DNA. The amount of ssDNA is also sufficient for partial ATR activation, as indicated by Rad17 phosphorylation. We hypothesize that only in the presence of higher levels of ssDNA is ATR fully activated and Chk1 phosphorylated, in keeping with the fact that Chk1 phosphorylation depends on the formation of long ssDNA gaps (50). Polyamide treatment also induced much lower levels of ATR T1989

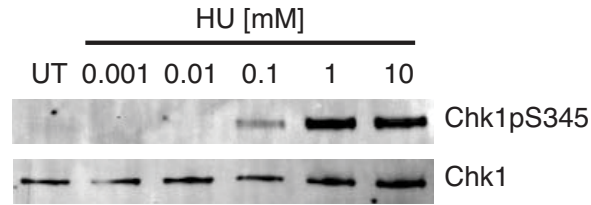


Figure 2.15 Dose-dependent increase in hydroxyurea (HU)-induced Chk1 S345 phosphorylation. Chk1 S345 phosphorylation was measured in DU145 cells treated with increasing doses of HU for 2 h. Chk1 S345 is maximally phosphorylated at 1 mM or higher HU.

phosphorylation than did HU treatment. This correlates as well with the lack of Chk1 phosphorylation, which requires robust ATR T1989 autophosphorylation (24,25), and is consistent with a model for quantitative regulation of ATR (25). ATR T1989 phosphorylation has actually been shown to be dispensable for ATR recruitment, Rad17 S645 phosphorylation, and recovery from transient replication stress (24,25). Based on these data, we conclude that ATR-MCM2 and FANCD2 signaling are sufficient to induce some fork protection. However, ATR-Chk1 cell cycle checkpoint activation requires ssDNA accumulation and extensive ATR T1989 phosphorylation, which is observed under higher replication stress (Figure 2.14B). While it is unclear what causes ssDNA accumulation and ATR-Chk1 activation, some possible causes are uncoupling of polymerase and helicase, accumulation of excess primers, or nascent DNA degradation.

A few studies have shown previously that the FA/BRCA pathway and the ATR-Chk1 pathway serve non-redundant functions and that their signaling mechanisms are separable. In human primary fibroblasts, Chk1 and FANCD2 both contribute to senescence induction but Chk1 is also responsible for persistent cell cycle arrest in response to psoralen treatment (51). Similarly, knockdown of FANCD2 but not Chk1 sensitizes HeLa cells to cisplatin treatment, despite activation of Chk1 (52). Supporting

the evidence for their different functions, it has been shown that the canonical ATR activators, Rad17 and TopBP1, are necessary for Chk1 phosphorylation but dispensable for FANCD2 monoubiquitination and FANCI phosphorylation in DT40 cells treated with MMC (53). Conversely, the FA core complex is necessary for FANCD2 monoubiquitination but is dispensable for Chk1 phosphorylation (53). Also, the interaction of FANCD2 with the MCMs is not dependent on Chk1 activity (40). Thus, the activation of the FA/BRCA pathway but not Chk1 in response to polyamide treatment appears to reflect a level of stress that does not require intervention by Chk1.

Hairpin Py-Im polyamide-induced replication stress causes what appears to be an intermediate state of ATR-dependent checkpoint response. We suggest that this is due to transient inhibition of replisome progression caused by the polyamide's unique high affinity non-covalent DNA-binding properties. This proposed mode of action distinguishes hairpin Py-Im polyamides from other replication inhibitors such as HU and aphidicolin, and will prove useful for further dissociating the S-phase, essential ATR functions from G2 checkpoint functions. Further delineation of the S-phase specific ATR mediators and effectors involved in protecting replication forks can be determined as distinct from or coordinated with those involved in cell cycle slowing.

2.4 Materials and Methods

Chemicals and reagents.

Hairpin Py-Im polyamides **1** and **2** were synthesized on solid phase Kaiser oxime resin using previously published protocols (54). Gemcitabine, etoposide, hydroxyurea,

and doxorubicin were purchased from Sigma-Aldrich, as were all other reagents unless otherwise noted.

Antibodies purchased from Santa Cruz Biotech were mouse anti-PCNA, anti-Chk1, anti-RPA2, anti-Rad17, anti-FANCD2, goat anti-ATR, and rat anti-BrdU (CldU cross-reactivity). Antibodies purchased from Bethyl were rabbit anti-H2AX, anti-MCM2, anti-MCM2pS108, and anti-RPA2pS4/S8. Antibodies purchased from Abcam were: rabbit anti-FANCD2, anti-MCM2pS108, anti-Rad9, anti-RPA2pS33, anti-Chk2, anti-H2AXpS139. Antibodies purchased from Cell Signaling Technologies were rabbit anti-ATMpS1981, anti-Rad17pS645, anti-Chk1pS345, anti-Chk1pS317, anti-Chk1pS296. Rabbit anti-Chk2pT68 was purchased from Millipore. Rabbit anti-ATM was purchased from Calbiochem. Rabbit anti-ATRpT1989 was a gift of Prof. Lee Zou.

Cell culture conditions.

LNCaP, LNAR, and DU145 cells were maintained in RPMI 1640 (Invitrogen) with 10% FBS (Irvine Scientific) at 37 °C under 5% CO₂. LNCaP and DU145 cells were purchased from ATCC (Manassas, VA). LNAR cells were a gift from C.L. Sawyers at Memorial Sloan-Kettering Cancer Center (NY, NY).

Cytotoxicity assay.

C₅₀ values for cytotoxicity were determined using a sulfarhodamine-based colorimetric assay for cellular protein content in 96-well microplates (55). LNCaP and LNAR cells were plated at 3,000 or 4,000 cells per well for the 72 h and 96 h time points,

respectively. DU145 cells were plated at 2,000 or 2,500 cells per well. Polyamides were added in 100 μ l RPMI 1640 supplemented with 10% FBS 24 h after plating. Quadruplicate wells were used for each concentration. Cells were fixed with 100 μ l 10% trichloroacetic acid solution, washed, stained, and dried as described. After solubilization of the bound dye in 10 mM Tris (pH 8), the absorbance was measured at 490 nm on a Victor microplate reader (PerkinElmer).

The cytotoxicity data are charted as a percentage of untreated controls, corrected for background absorbance. IC_{50} is defined as the concentration that inhibits 50% of control cell growth. These values were determined by non-linear least squares regression fit to $Y = A + (B-A)/(1+10^{((\text{Log } EC_{50}-X)*H})}$, where A =max, B =min, and H =Hill Slope. Three independent trials were averaged; stated IC_{50} values represent the mean and standard deviation. These calculations were performed using Prism 4 (GraphPad) software.

Caspase 3/7 activation assay.

DU145 cells were plated in 96-well microplates at 2,000-8,000 cells per well. As above, polyamides and controls were added 24 h after plating. Each timepoint was assayed in triplicate. At harvest, Caspase 3/7 activity was assessed using 100 μ l of Caspase-Glo reagent (Promega), which contains the proluminescent caspase substrate DEVD-aminoluciferin. Luminescence was measured after 30 min incubation at room temperature. Luminescence data are expressed as a fold difference from untreated controls as measured using a Victor microplate reader (PerkinElmer). The cell viability of

each treatment condition was monitored in a sister plate using a tetrazolium-based assay for mitochondrial bio-reductive capacity (56). 10 μ l WST-1 reagent (Roche) was added to each well and incubated at 37 °C for 30 min before measuring the absorbance at 450 nm. The WST-1 data are corrected for background absorbance and expressed as a percentage of untreated controls.

PARP cleavage assay.

400,000 DU145 cells were plated in 10 cm diameter dishes. Polyamides were added after 24 h and were allowed to incubate an additional 72 h. At harvest, cells were washed once with PBS then treated with 400 μ l ice-cold lysis buffer (20 mM Tris-HCl pH 7.5, 150 mM NaCl, 1 mM Na₂EDTA, 1 mM EGTA, 1% Triton, 2.5 mM sodium pyrophosphate, 2 mM β -glycerophosphate, 1 mM Na₃VO₄, 1 μ g/ml leupeptin, 1 mM PMSF) for 5 min at 5°C. The lysate was sonicated for 15 s and then centrifuged for 10 min at 20,000 x g at 5°C. The supernatant was retained. Protein concentrations were determined by Bradford assay (Bio-Rad) using bovine serum albumin (Bio-Rad) to create a standard curve. PARP cleavage was assayed by sandwich ELISA (Cell Signaling Technology) and performed according to the manufacturer's recommendations. 10 μ g total protein was loaded into each well of a microplate coated with anti-cleaved PARP (Asp214) mouse mAb and allowed to incubate overnight at 5°C. Rabbit anti-PARP mAb was then added, followed by anti-rabbit IgG conjugated to HRP. Triplicate wells were included for each condition, and the data are representative of both experimental replicates. The data are expressed as fold change from the untreated condition, showing the mean and standard deviation of each measurement.

Cell cycle analysis.

800,000 DU145 cells were plated in 10 cm diameter dishes for 24 h before treatment with polyamides for an additional 24 h. Cells were pulsed with 10 μ M EdU 30 min before harvest to estimate rate of DNA synthesis. Cells were trypsinized and pelleted at 300 x g with cell culture supernatant. Following overnight fixation in 70% ethanol, the cells were rehydrated in 1% BSA/PBS and processed with the Click-it EdU Alexa Fluor 488 Flow Cytometry assay kit (Invitrogen) using half the recommended A488 reagent. After overnight treatment with 0.2 mg/ml RNase A in 1% BSA/PBS, the cells were stained for DNA content with 7-aminoactinomycin D and analyzed on a FACSCalibur (Becton-Dickinson) instrument. The data were analyzed using FlowJo v9.5.3 (TreeStar) and are representative of two trials. Monoparametric, propidium iodide, flow cytometry was also used to evaluate the effect of polyamides **1** and **2** on cell cycle distribution. DU145 cells were treated with 1-100 μ M of polyamide **1** or 0.1-10 μ M of polyamide **2** for 48 h. The effect of PI3 kinases on cell cycle distribution was measured by treating DU145 cells with 10 μ M polyamide **1** or 1 μ M polyamide **2** as well as 2 mM caffeine, 4 or 10 μ M NU6027 (Calbiochem) and 4 or 10 μ M KU55933 (Calbiochem) for 36 h. Data were analyzed using FlowJo and fitted to the Watson (Pragmatic) model. The data are representative of two trials.

Knockdown of ATR and FANCD2 by siRNA.

ATR was knocked down for cell cycle analysis and immunoblot experiments using 20 nM Silencer Select siRNA against ATR (Ambion, s536) and RNAiMAX

lipofectamine (Life Technologies) according to the manufacturer's protocol. 20 nM Silencer Select Negative Control #1 (Ambion) was used as a control. FANCD2 was knocked down using 25 nM Dharmacon SMARTpool, siGENOME Human FANCD2 (2177). 25 nM siGENOME Non-Targeting Pool #1 was used as a control. Briefly, the siRNA was incubated for 48 h, with a media swap after the first 24 h, prior to the addition of 10 μ M polyamide **1** or 1 μ M polyamide **2** for an additional 36 h. Efficiency of knockdown was determined by western blot.

PCNA (Proliferating Cell Nuclear Antigen) immunocytochemistry.

PCNA immunocytochemistry experiments were performed as in (23). Briefly, DU145 cells were plated in 4-well glass chamber slides (Lab-Tek) at 70,000 cells per well. Polyamide **1** was added at a final concentration of 10 μ M and polyamide **2** at a final concentration of 1 μ M with 0.2% DMSO. After fixation, permeabilization, and blocking, cells were incubated with mouse PCNA mAb at a 1:500 dilution at 4°C overnight. Cells were then washed, followed by incubation with Alexa Fluor 488-conjugated donkey anti-mouse IgG (Life Technologies) at a 1:400 dilution at room temperature for 2 h. Cells were washed and mounted with Prolong Gold Anti-Fade reagent with DAPI (Life Technologies). Images were obtained using a Zeiss LSM 510 Meta NLO with Coherent Chameleon and a Plan-Apochromat 63x 1.4-numerical aperture oil immersion objective lens and processed using the LSM Browser software package. Foci were counted using the open source Python software, FociCounter (<http://focicounter.sourceforge.net/>). Parameters were kept constant across all conditions for a particular replicate, but differed slightly over the three replicates to account for differences in staining. Cells that were

likely positive but sufficiently out of focus so as to not produce distinct foci were not counted. Kruskal-Wallis test was performed using Prism 4 (Graphpad) software.

Assessment of phosphorylation of proteins by immunoblot.

800,000 DU145 cells were plated in 10 cm diameter dishes and allowed to adhere for 24 h before treatment with 0.1% DMSO, polyamide **1**, or polyamide **2** for the indicated time. Cells were lysed in TBS-Tx buffer (50 mM Tris-HCl pH 7.4, 150 mM NaCl, 1 mM EDTA, 1% Triton X-100) containing fresh protease inhibitors (Roche), 1 mM PMSF, phosphatase inhibitors, and 10 mM N-ethylmaleimide. The samples were quantified by Bradford assay, denatured by boiling in Laemmli buffer, and total protein was separated by SDS-PAGE on 4-15% gradient polyacrylamide gels (Bio-rad). After transfer to the nitrocellulose (Bio-rad) or PVDF (Millipore) membrane and blocking with Odyssey Blocking Buffer (Li-Cor), primary antibodies were incubated overnight at 4°C. Donkey anti-rabbit, Donkey anti-mouse, or donkey anti-goat 800CW IR dye-conjugated secondary antibody (Li-Cor) was added and the bands were visualized on an Odyssey infrared imager (Li-Cor). For assessment of MCM2 and FANCD2 modification, plates treated with either DMSO, polyamide **1**, polyamide **2**, or polyamide plus 2 mM caffeine, 10 μ M KU55933 (KU, ATM inhibitor), or 10 μ M NU6027 (NU, ATR inhibitor) were added together and harvested at the indicated times. For hydroxyurea (HU) treatment, cells were incubated with the indicated inhibitor for 34 h prior to the addition of HU for the final 2 h before harvesting at 36 h. ATR immunoprecipitation was performed using pre-cleared Protein G agarose beads (Pierce) and either normal goat IgG or ATR (N19)

antibodies (Santa Cruz) overnight at 4°C. All immunoblots and accompanying quantifications are representative of at least two biological replicates.

Chromatin fractionation assay.

2 x 10⁶ DU145 cells were plated in 15 cm diameter dishes and allowed to adhere for 24 h, followed by treatment with 0.1% DMSO, 10 μM polyamide **1**, 1 μM polyamide **2**, or 10 mM HU for indicated times. Chromatin fractions were prepared according to published protocols(57). Briefly, cells were harvested, washed with PBS, and resuspended with 400 μL buffer A (10 mM HEPES pH 7.9, 10 mM KCl, 1.5 mM MgCl₂, 0.34M sucrose, 10% glycerol, 1 mM DTT, and fresh protease and phosphatase inhibitors). Triton X-100 was added to a final concentration of 0.1% and incubated on ice for 5 min followed by centrifugation at 1,300 x g for 4 min to pellet the nuclei. Nuclei were washed with buffer A and then lysed with 400 μL buffer B (3 mM EDTA, 0.2 mM EGTA, 1 mM DTT) for 10 min on ice. Chromatin was pelleted by centrifugation at 1,700 x g for 4 min. Isolated chromatin was washed once with buffer B and spun down at 10,000 x g for 1 min. The supernatant is completely removed and the chromatin pellet was resuspended in 300 μL SDS sample buffer and sheared for 20 s at 25% amplitude with a microtip adapter. Samples were then incubated at 80°C and analyzed by SDS-PAGE and immunoblot.

5-chloro-2'-deoxyuridine immunocytochemistry.

20,000 or 50,000 DU145 cells were plated in 4-well glass chamber slides and allowed to adhere for 24 h. Cells were incubated with 50 μM CldU for 48 h then the

media was swapped and polyamide added. Following polyamide treatment, cells were washed, fixed with 2% formaldehyde (Ted Pella), and permeabilized with 0.2% Triton X-100. Following permeabilization, cells were blocked with 3% goat serum with 0.1% Triton for 45 min at room temperature. After blocking, cells were washed with 0.1% Triton and then incubated with rat anti-BrdU antibody (ICR1) at a concentration of 10 $\mu\text{g}/\text{mL}$ in 3% goat serum for 30 min at 37°C. After washes, cells were incubated with chicken anti-rat Alexa488 antibody at a concentration of 4 $\mu\text{g}/\text{mL}$. Finally, cells were washed, mounted, and then imaged as in PCNA staining above. Cells were scored as positive for ssDNA if >10 foci were counted. 150 cells were counted per condition over three biological replicates.

Single cell alkaline gel electrophoresis.

The apparatus and reagent kit were purchased from Trevigen. The assay was performed according to the manufacturer's recommendations. Briefly, 800,000 DU145 cells were plated in 10 cm diameter dishes for 24 h before treatment with polyamides for an additional 36 h. Cells were harvested by trypsinization and washed once with cold PBS before being suspended in 37°C low-melting point agarose at 1×10^5 cells/ml. An aliquot of the suspension was placed on a 37°C glass slide and allowed to cool for 30 min. The slides were bathed in lysis buffer for 30 min followed by a 30 min treatment with alkaline unwinding buffer (200 mM NaOH, 1 mM EDTA) at 5°C. The slides were subjected to electrophoresis at 21V in a prechilled apparatus and fresh unwinding buffer for 30 min. The slides were washed twice in water and once in 70% ethanol, then dried for 30 min. at 37 °C. Dried slides were stained with 1X SYBR Gold in TE buffer for 30

min at room temperature, and excess dye was removed by blotting. Slides were dried and stored at room temperature with desiccant. Comets were visualized using a Zeiss LSM 510 Meta NLO confocal microscope with a 5x objective (Zeiss) and scored using Comet Assay IV image analysis software (Perceptive). A random sampling of 400 cells from two biological replicates were analyzed for each condition. The data are displayed as a box and whisker diagram showing median and middle quartiles with whiskers at the min and max.

T7 gp4A helicase assays.

Helicase assays using T7 gp4A (BioHelix) were performed as published in (45). First, 40 pmol of a 75mer oligonucleotide was labeled with [γ - 32 P]ATP (MP Biomedicals) using T4 polynucleotide kinase (NEB) and annealed to 80 pmol of a 95mer oligonucleotide with 56 complementary bases to form a forked substrate in STE buffer (100 mM NaCl, 10 mM Tris-HCl, 1 mM EDTA). The forked substrate was purified by extraction from a 10% non-denaturing acrylamide gel. To assess polyamide effects on gp4A helicase activity, the forked substrate (1:1000 dilution final) was incubated in a 10 μ l volume with increasing concentrations of polyamide **1** (DMSO solution, 5% final concentration) in 1x reaction buffer (BioHelix) for 1 h at room temperature prior to addition of gp4A at a final concentration 143 ng/ml (\sim 2.27 nM) and incubated at 30°C for 10 min. The mock treated helicase reaction contained 5% DMSO with no polyamide. Reactions were stopped with the addition of 5 μ l stop buffer (60 mM EDTA, 40% sucrose, 0.6% SDS, 0.25% bromphenol blue, and 0.25% xylene cyanole FF). Unwound labeled single-stranded 75mer was separated from the intact fork substrate on a pre-run

10% non-denaturing acrylamide gel at 200 V for 1 h. The gel was then placed on a PhosphorImager screen (Molecular Dynamics) overnight and imaged on a Storm Molecular Imager. Match 75mer: 5'-CGC CGG GTA CCG AGC TCG AAT TCA CTG GCC GTC GTT TTA CAA CGT CGT **GAA CTG** CCT₁₉-3'. Match 95mer: 5'-T₃₉GGC **AGT TCA** CGA CGT TGT AAA ACG ACG GCC AGT GAA TTC GAG CTC GGT ACC CGG CG-3'. Mismatch 75mer: 5'-CGC CGG GTA CCG AGC TCG AAT TCA CTG GCC GTC GTT TTA CAA CGT CGT **GAC ATG** CCT₁₉-3'. Mismatch 95mer: 5'-T₃₉GGC **ATG TCA** CGA CGT TGT AAA ACG ACG GCC AGT GAA TTC GAG CTC GGT ACC CGG CG-3'.

S. cerevisiae Dna2-K677R helicase assay.

S. cerevisiae K677R Dna2 (yDna2-K677R), lacking nuclease activity, was prepared and helicase assays were performed similarly to (58). First, 40 pmol of a 42mer oligonucleotide was labeled with [γ -³²P]ATP (MP Biomedicals) and annealed to 80 pmol of a 29mer oligonucleotide with 24 complementary bases to form a forked substrate in STE buffer. To assess polyamide effects on yDna2-K677R helicase activity, the forked substrate (1:2000 dilution final) was incubated in a 20 μ l volume with increasing concentrations of polyamide **1** (DMSO solution, 5% final concentration) in 1x reaction buffer (25 mM Tris-HCl (pH 7.5), 2 mM MgCl₂, 2 mM DTT, 0.25 mg/ml BSA, 2 mM ATP) for 1 h at room temperature prior to addition of 150 fmol yDna2-K667R and incubated at 37°C for 30 min. The mock treated helicase reaction contained 5% DMSO with no polyamide. Reactions were stopped with the addition of 5 μ l stop buffer. Unwound labeled single-stranded 42mer was separated from the intact fork substrate on a

pre-run 20% non-denaturing acrylamide gel run at 150 V for 3 h. The gel was then placed on a PhosphorImager screen overnight and imaged on a Storm Molecular Imager. Match 42mer: 5'-AGC TAG CTC TTG ATC GTG ACG **AGA ACA** CCA GAA CGA GTA GTA-3'. Match 29mer 5'-TAC TAC TCG TTC TGG **TGT TCT** CGT TGA TC-3'. Mismatch 42mer: 5'-AGC TAG CTC TTG ATC GTG ACG **AGA AAA** CCA GAA CGA GTA GTA-3'. Mismatch 29mer 5'-TAC TAC TCG TTC TGG **TTT TCT** CGT TGA TC-3'.

S. cerevisiae Dna2-K677R ATPase Assay.

The ATPase assay was run as in (58). Briefly, reactions containing 300 fmol of yDna2-K677R protein in 20 μ l of reaction buffer (40 mM Tris-HCl (pH 7.5), 5 mM MgCl₂, 25 mM NaCl, 1 mM DTT, 0.5 mg/ml BSA, 0.2 mM ATP, 10% glycerol, and 3 μ Ci of [γ -³²P]ATP) were supplemented with the mismatch 42mer plus DMSO or 3 μ M polyamide **1** and incubated at 30 °C for 1 h. The reactions were stopped by addition of EDTA. 0.8 μ l of each reaction was spotted onto a polyethyleneimine-cellulose TLC plate (Selecto Scientific) and developed in 0.5 M LiCl, 1 M formic acid solution. The radiolabelled products were detected by PhosphorImager.

Clonogenic assays.

Clonogenic assays were performed with FANCD2-deficient PD20 cells complemented with empty vector (PD20-EV) or FANCD2 (PD20-FANCD2). FANCD2 protein expression and phenotype rescue was previously confirmed (59). Briefly, 1000 cells per well were seeded in a 12 well plate and left to attach overnight. Polyamide **1** (0, 10, 20, 30 μ M) or polyamide **2** (0, 1, 2, 3 μ M) was added for 36 h. Polyamide-containing

media was exchanged for fresh media and cells were cultured for 14 days with media changed every 4 days. Visible colonies were fixed and stained with 1% crystal violet in methanol and enumerated. Three independent experiments were performed.

2.5 Acknowledgments

We thank Dr. Subhash Pokharel for *S. cerevisiae* Dna2-K677R, C. L. Sawyers (University of California, Los Angeles) for the LNAR cell line, and L. Zou for the ATRpT1989 antibody (Harvard Medical School). We thank members of the Dervan and Campbell laboratories for critical reading of the manuscript. We thank members of the Dunphy laboratory for helpful discussions. Mass spectrometry analyses were performed in the Mass Spectrometry Laboratory of the Division of Chemistry and Chemical Engineering at the California Institute of Technology. Imaging was performed at the Caltech Bioimaging Center in the Beckman Institute. Flow cytometry analyses were performed at the Caltech Flow Cytometry Cell Sorting Facility. We thank Rochelle Diamond for support and technical expertise in performing flow cytometry experiments. This work was supported by the National Institutes of Health [R01GM27681 and R01GM51747 to P.B.D., R01GM07866 to J.L.C.]; the Ellison Foundation [AG-SS-2143-08 to J.L.C.]; the Margaret Early Trust [to J.L.C.], the Army Research Office [09-1-0041 to J.L.C.]; T.F.M. is a recipient of a predoctoral fellowship [F31CA159896] from the National Institutes of Health.

2.6 References

1. Ciccia, A. and Elledge, S.J. (2010) The DNA Damage Response: Making It Safe to Play with Knives. *Mol. Cell*, 40, 179-204.
2. Branzei, D. and Foiani, M. (2008) Regulation of DNA repair throughout the cell cycle. *Nat. Rev. Mol. Cell Biol.*, 9, 297-308.
3. Olson, E., Nievera, C.J., Klimovich, V., Fanning, E. and Wu, X. (2006) RPA2 is a direct downstream target for ATR to regulate the S-phase checkpoint. *J. Biol. Chem.*, 281, 39517-39533.
4. Cimprich, K.A. and Cortez, D. (2008) ATR: an essential regulator of genome integrity. *Nat. Rev. Mol. Cell Biol.*, 9, 616-627.
5. Polo, S.E. and Jackson, S.P. (2011) Dynamics of DNA damage response proteins at DNA breaks: a focus on protein modifications. *Genes Dev.*, 25, 409-433.
6. Zeman, M.K. and Cimprich, K.A. (2014) Causes and consequences of replication stress. *Nat. Cell Biol.*, 16, 2-9.
7. Trauger, J.W., Baird, E.E. and Dervan, P.B. (1996) Recognition of DNA by designed ligands at subnanomolar concentrations. *Nature*, 382, 559-561.
8. White, S., Szewczyk, J.W., Turner, J.M., Baird, E.E. and Dervan, P.B. (1998) Recognition of the four Watson-Crick base pairs in the DNA minor groove by synthetic ligands. *Nature*, 391, 468-471.
9. Chenoweth, D.M. and Dervan, P.B. (2010) Structural basis for cyclic Py-Im polyamide allosteric inhibition of nuclear receptor binding. *J. Am. Chem. Soc.*, 132, 14521-14529.
10. Edelson, B.S., Best, T.P., Olenyuk, B., Nickols, N.G., Doss, R.M., Foister, S., Heckel, A. and Dervan, P.B. (2004) Influence of structural variation on nuclear localization of DNA-binding polyamide-fluorophore conjugates. *Nucleic Acids Res.*, 32, 2802-2818.
11. Luck, G., Zimmer, C., Reinert, K.E. and Arcamone, F. (1977) Specific interactions of distamycin A and its analogs with (A-T) rich and (G-C) rich duplex regions of DNA and deoxypolynucleotides. *Nucleic Acids Res.*, 4, 2655-2670.
12. Baraldi, P.G., Beria, I., Cozzi, P., Bianchi, N., Gambari, R. and Romagnoli, R. (2003) Synthesis and growth inhibition activity of alpha-bromoacrylic heterocyclic and benzoheterocyclic derivatives of distamycin A modified on the amidino moiety. *Bioorg. Med. Chem.*, 11, 965-975.

13. Zimmer, C., Puschendorf, B., Grunicke, H., Chandra, P. and Venner, H. (1971) Influence of netropsin and distamycin A on the secondary structure and template activity of DNA. *Eur. J. Biochem.*, 21, 269-278.
14. Beerman, T.A., McHugh, M.M., Sigmund, R., Lown, J.W., Rao, K.E. and Bathini, Y. (1992) Effects of analogs of the DNA minor groove binder Hoechst-33258 on Topoisomerase-II and Topoisomerase-I mediated activities. *Biochim. Biophys. Acta*, 1131, 53-61.
15. Brosh, R.M., Jr., Karow, J.K., White, E.J., Shaw, N.D., Hickson, I.D. and Bohr, V.A. (2000) Potent inhibition of werner and bloom helicases by DNA minor groove binding drugs. *Nucleic Acids Res.*, 28, 2420-2430.
16. Nickols, N.G. and Dervan, P.B. (2007) Suppression of androgen receptor-mediated gene expression by a sequence-specific DNA-binding polyamide. *Proc. Natl. Acad. Sci. USA*, 104, 10418-10423.
17. Yang, F., Nickols, N.G., Li, B.C., Marinov, G.K., Said, J.W. and Dervan, P.B. (2013) Antitumor activity of a pyrrole-imidazole polyamide. *Proc. Natl. Acad. Sci. USA*, 110, 1863-1868.
18. Roche, P.J., Hoare, S.A. and Parker, M.G. (1992) A consensus DNA-binding site for the androgen receptor. *Mol. Endocrinol.*, 6, 2229-2235.
19. Chenoweth, D.M., Harki, D.A., Phillips, J.W., Dose, C. and Dervan, P.B. (2009) Cyclic pyrrole-imidazole polyamides targeted to the androgen response element. *J. Am. Chem. Soc.*, 131, 7182-7188.
20. Xu, Y.Y., Chen, S.Y., Ross, K.N. and Balk, S.P. (2006) Androgens induce prostate cancer cell proliferation through mammalian target of rapamycin activation and post-transcriptional increases in cyclin D proteins. *Cancer Res.*, 66, 7783-7792.
21. Alimirah, F., Chen, J., Basrawala, Z., Xin, H. and Choubey, D. (2006) DU-145 and PC-3 human prostate cancer cell lines express androgen receptor: implications for the androgen receptor functions and regulation. *FEBS Lett.*, 580, 2294-2300.
22. Essers, J., Theil, A.F., Baldeyron, C., van Cappellen, W.A., Houtsmuller, A.B., Kanaar, R. and Vermeulen, W. (2005) Nuclear dynamics of PCNA in DNA replication and repair. *Mol. Cell. Biol.*, 25, 9350-9359.
23. Aggarwal, M., Sommers, J.A., Shoemaker, R.H. and Brosh, R.M., Jr. (2011) Inhibition of helicase activity by a small molecule impairs Werner syndrome helicase (WRN) function in the cellular response to DNA damage or replication stress. *Proc. Natl. Acad. Sci. USA*, 108, 1525-1530.

24. Nam, E.A., Zhao, R.X., Glick, G.G., Bansbach, C.E., Friedman, D.B. and Cortez, D. (2011) Thr-1989 Phosphorylation Is a Marker of Active Ataxia Telangiectasia-mutated and Rad3-related (ATR) Kinase. *J. Biol. Chem.*, 286, 28707-28714.
25. Liu, S.Z., Shiotani, B., Lahiri, M., Marechal, A., Tse, A., Leung, C.C.Y., Glover, J.N.M., Yang, X.H.H. and Zou, L. (2011) ATR Autophosphorylation as a Molecular Switch for Checkpoint Activation. *Mol. Cell*, 43, 192-202.
26. Peasland, A., Wang, L.Z., Rowling, E., Kyle, S., Chen, T., Hopkins, A., Cliby, W.A., Sarkaria, J., Beale, G., Edmondson, R.J. *et al.* (2011) Identification and evaluation of a potent novel ATR inhibitor, NU6027, in breast and ovarian cancer cell lines. *Br. J. Cancer*, 105, 372-381.
27. So, S.R., Davis, A.J. and Chen, D.J. (2009) Autophosphorylation at serine 1981 stabilizes ATM at DNA damage sites. *J. Cell Biol.*, 187, 977-990.
28. Bao, S.D., Tibbetts, R.S., Brumbaugh, K.M., Fang, Y.N., Richardson, D.A., Ali, A., Chen, S.M., Abraham, R.T. and Wang, X.F. (2001) ATR/ATM-mediated phosphorylation of human Rad17 is required for genotoxic stress responses. *Nature*, 411, 969-974.
29. Kozlov, S.V., Graham, M.E., Jakob, B., Tobias, F., Kijas, A.W., Tanuji, M., Chen, P., Robinson, P.J., Taucher-Scholz, G., Suzuki, K. *et al.* (2011) Autophosphorylation and ATM activation: additional sites add to the complexity. *J. Biol. Chem.*, 286, 9107-9119.
30. Hickson, I., Zhao, Y., Richardson, C.J., Green, S.J., Martin, N.M., Orr, A.I., Reaper, P.M., Jackson, S.P., Curtin, N.J. and Smith, G.C. (2004) Identification and characterization of a novel and specific inhibitor of the ataxia-telangiectasia mutated kinase ATM. *Cancer Res.*, 64, 9152-9159.
31. Liu, S.Q., Opiyo, S.O., Manthey, K., Glanzer, J.G., Ashley, A.K., Amerin, C., Troksa, K., Shrivastav, M., Nickoloff, J.A. and Oakley, G.G. (2012) Distinct roles for DNA-PK, ATM and ATR in RPA phosphorylation and checkpoint activation in response to replication stress. *Nucleic Acids Res.*, 40, 10780-10794.
32. Okita, N., Minato, S., Ohmi, E., Tanuma, S. and Higami, Y. (2012) DNA damage-induced CHK1 autophosphorylation at Ser296 is regulated by an intramolecular mechanism. *FEBS Lett.*, 586, 3974-3979.
33. Vassin, V.M., Anantha, R.W., Sokolova, E., Kanner, S. and Borowiec, J.A. (2009) Human RPA phosphorylation by ATR stimulates DNA synthesis and prevents ssDNA accumulation during DNA-replication stress. *J. Cell Sci.*, 122, 4070-4080.
34. Ward, I.M., Wu, X.L. and Chen, J.J. (2001) Threonine 68 of Chk2 is phosphorylated at sites of DNA strand breaks. *J. Biol. Chem.*, 276, 47755-47758.

35. Pabla, N., Huang, S., Mi, Q.S., Daniel, R. and Dong, Z. (2008) ATR-Chk2 signaling in p53 activation and DNA damage response during cisplatin-induced apoptosis. *J. Biol. Chem.*, 283, 6572-6583.
36. Sirbu, B.M., Couch, F.B., Feigerle, J.T., Bhaskara, S., Hiebert, S.W. and Cortez, D. (2011) Analysis of protein dynamics at active, stalled, and collapsed replication forks. *Genes Dev.*, 25, 1320-1327.
37. Fragkos, M., Jurvansuu, J. and Beard, P. (2009) H2AX Is Required for Cell Cycle Arrest via the p53/p21 Pathway. *Mol. Cell. Biol.*, 29, 2828-2840.
38. Yoo, H.Y., Shevchenko, A. and Dunphy, W.G. (2004) Mcm2 is a direct substrate of ATM and ATR during DNA damage and DNA replication checkpoint responses. *J. Biol. Chem.*, 279, 53353-53364.
39. Trenz, K., Errico, A. and Costanzo, V. (2008) Plx1 is required for chromosomal DNA replication under stressful conditions. *EMBO J.*, 27, 876-885.
40. Lossaint, G., Larroque, M., Ribeyre, C., Bec, N., Larroque, C., Decaillet, C., Gari, K. and Constantinou, A. (2013) FANCD2 binds MCM proteins and controls replisome function upon activation of s phase checkpoint signaling. *Mol. Cell*, 51, 678-690.
41. Shigechi, T., Tomida, J., Sato, K., Kobayashi, M., Eykelenboom, J.K., Pessina, F., Zhang, Y., Uchida, E., Ishiai, M., Lowndes, N.F. *et al.* (2012) ATR-ATRIP kinase complex triggers activation of the Fanconi anemia DNA repair pathway. *Cancer Res.*, 72, 1149-1156.
42. Schlacher, K., Wu, H. and Jasin, M. (2012) A distinct replication fork protection pathway connects Fanconi anemia tumor suppressors to RAD51-BRCA1/2. *Cancer Cell*, 22, 106-116.
43. Andreassen, P.R., D'Andrea, A.D. and Taniguchi, T. (2004) ATR couples FANCD2 monoubiquitination to the DNA-damage response. *Genes Dev.*, 18, 1958-1963.
44. Kennedy, R.D., Chen, C.C., Stuckert, P., Archila, E.M., De la Vega, M.A., Moreau, L.A., Shimamura, A. and D'Andrea, A.D. (2007) Fanconi anemia pathway-deficient tumor cells are hypersensitive to inhibition of ataxia telangiectasia mutated. *J. Clin. Invest.*, 117, 1440-1449.
45. Satapathy, A.K., Kulczyk, A.W., Ghosh, S., van Oijen, A.M. and Richardson, C.C. (2011) Coupling dTTP hydrolysis with DNA unwinding by the DNA helicase of bacteriophage T7. *J. Biol. Chem.*, 286, 34468-34478.
46. Dose, C., Farkas, M.E., Chenoweth, D.M. and Dervan, P.B. (2008) Next generation hairpin polyamides with (R)-3,4-diaminobutyric acid turn unit. *J. Am. Chem. Soc.*, 130, 6859-6866.

47. Koundrioukoff, S., Carignon, S., Techer, H., Letessier, A., Brison, O. and Debatisse, M. (2013) Stepwise Activation of the ATR Signaling Pathway upon Increasing Replication Stress Impacts Fragile Site Integrity. *PLoS Genet.*, 9, e1003643.
48. Sirbu, B.M., McDonald, W.H., Dungrawala, H., Badu-Nkansah, A., Kavanaugh, G.M., Chen, Y., Tabb, D.L. and Cortez, D. (2013) Identification of proteins at active, stalled, and collapsed replication forks using isolation of proteins on nascent DNA (iPOND) coupled with mass spectrometry. *J. Biol. Chem.*, 288, 31458-31467.
49. Ishiai, M., Kitao, H., Smogorzewska, A., Tomida, J., Kinomura, A., Uchida, E., Saberi, A., Kinoshita, E., Kinoshita-Kikuta, E., Koike, T. *et al.* (2008) FANCI phosphorylation functions as a molecular switch to turn on the Fanconi anemia pathway. *Nat. Struct. Mol. Biol.*, 15, 1138-1146.
50. MacDougall, C.A., Byun, T.S., Van, C., Yee, M.C. and Cimprich, K.A. (2007) The structural determinants of checkpoint activation. *Genes Dev.*, 21, 898-903.
51. Hovest, M.G., Krieg, T. and Herrmann, G. (2011) Differential roles for Chk1 and FANCD2 in ATR-mediated signalling for psoralen photoactivation-induced senescence. *Experimental dermatology*, 20, 883-889.
52. Wagner, J.M. and Karnitz, L.M. (2009) Cisplatin-Induced DNA Damage Activates Replication Checkpoint Signaling Components that Differentially Affect Tumor Cell Survival. *Mol. Pharmacol.*, 76, 208-214.
53. Tomida, J., Itaya, A., Shigechi, T., Unno, J., Uchida, E., Ikura, M., Masuda, Y., Matsuda, S., Adachi, J., Kobayashi, M. *et al.* (2013) A novel interplay between the Fanconi anemia core complex and ATR-ATRIP kinase during DNA cross-link repair. *Nucleic Acids Res.*, 41, 6930-6941.
54. Belitsky, J.M., Nguyen, D.H., Wurtz, N.R. and Dervan, P.B. (2002) Solid-phase synthesis of DNA binding polyamides on oxime resin. *Bioorg. Med. Chem.*, 10, 2767-2774.
55. Vichai, V. and Kirtikara, K. (2006) Sulforhodamine B colorimetric assay for cytotoxicity screening. *Nature protocols*, 1, 1112-1116.
56. Ishiyama, M., Shiga, M., Sasamoto, K., Mizoguchi, M. and He, P.G. (1993) A New Sulfonated Tetrazolium Salt That Produces a Highly Water-Soluble Formazan Dye. *Chem. Pharm. Bull. (Tokyo)*, 41, 1118-1122.
57. Zou, L., Cortez, D. and Elledge, S.J. (2002) Regulation of ATR substrate selection by Rad17-dependent loading of Rad9 complexes onto chromatin. *Genes Dev.*, 16, 198-208.

58. Fortini, B.K., Pokharel, S., Polaczek, P., Balakrishnan, L., Bambara, R.A. and Campbell, J.L. (2011) Characterization of the endonuclease and ATP-dependent flap endo/exonuclease of Dna2. *J. Biol. Chem.*, 286, 23763-23770.
59. Karanja, K.K., Cox, S.W., Duxin, J.P., Stewart, S.A. and Campbell, J.L. (2012) DNA2 and EXO1 in replication-coupled, homology-directed repair and in the interplay between HDR and the FA/BRCA network. *Cell cycle*, 11, 3983-3996.